

Network mechanisms that represent novelty and familiarity in the medial Entorhinal Cortex (mEC)



Master's Thesis

Author:

Bharath Krishnan

BS-MS student
Roll no: 20131116
IISER, Pune

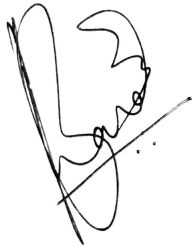
Supervisor:

Dr. Collins Assisi

Assistant Professor
Department of Biology
IISER, Pune

Certificate

This is to certify that this dissertation entitled “Network mechanisms that represent novelty and familiarity in the medial Entorhinal Cortex (mEC)” towards the partial fulfilment of the BS-MS dual degree programme at the Indian Institute of Science Education and Research, Pune represents study/work carried out by Bharath Krishnan at the Indian Institute of Science Education and Research, Pune under the supervision of Dr. Collins Assisi, Assistant Professor, Department of Biology, during the academic year 2017-2018.

A handwritten signature in black ink, appearing to be 'Bharath Krishnan', written in a cursive style.

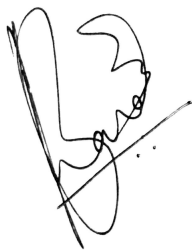
Bharath Krishnan

A handwritten signature in black ink, appearing to be 'Collins Assisi', written in a cursive style.

Dr. Collins Assisi

Declaration

I hereby declare that the matter embodied in the report entitled “Network mechanisms that represent novelty and familiarity in the medial Entorhinal Cortex (mEC)” are the results of the work carried out by me at the Department of Biology, Indian Institute of Science Education and Research, Pune, under the supervision of Dr. Collins Assisi and the same has not been submitted elsewhere for any other degree.

A handwritten signature in black ink, appearing to be 'Bharath Krishnan', written in a cursive style.

Bharath Krishnan

A handwritten signature in black ink, appearing to be 'Collins Assisi', written in a cursive style.

Dr. Collins Assisi

Acknowledgments

I would like to extend my deepest gratitude to my project mentor, Dr. Collins Assisi. His unwavering encouragement and guidance throughout the course of the project made it an absolute delight to work under his tutelage. Dr. Assisi's experience in modelling neuronal networks, and knowledge about Hippocampal and spatial navigation literature enabled me to learn a lot over the course of my Master's thesis. Regular weekly meetings, and group discussions with him helped me gain a deep understanding and appreciation for the study of the brain. I believe such meetings and discussions from a pivotal part, and contribute extensively to the holistic development of every student of Science. These interactions, in conjunction with a very conducive lab environment, would often help me find my way, when I would I be lost on a particular aspect of the problem.

I would like to thank Arun Neru, a final year PhD student in the lab, for his help with the project. Arun's work on Entorhinal Cortex circuits, and astute calibration of neuronal parameters such as channel conductance values, synaptic weights, synaptic gating variables, network architecture etc. allowed me to easily set-up my networks and start asking the exciting questions very early into the project. I would also like to thank Dr. Suhita Nadkarni, and other members of the Computational Neuroscience Lab for their helpful criticisms and suggestions during lab meetings. Their ideas and presence in the laboratory provided me with valuable insights from other subdisciplines of Neuroscience I knew very little about.

Finally, I am extremely thankful to the people who have kept me company outside the confines of the laboratory - my friends and parents. Light-hearted discussions at home and the occasional hunt for delicacies at Pune's restaurants has made for many fond memories over the past 10 months - things that I'll be cherishing for times to come.

Abstract

Grid cells in the medial entorhinal cortex (mEC) fire action potentials whenever the animal is positioned at the vertices of a tessellating hexagonal grid. Changes to the animal's environment can alter grid orientation, break its symmetry along specific axes, and increase or decrease the spatial scale of the grid. In this work, we focus on a transformation of the spatial scale of the grid as a function of the novelty of the environment. The grid pattern formed by an individual grid cell shows visible changes in novel environments - its hexagonal symmetry is distorted, and there is an increase in the spatial scale of the entire grid. As the animal spends more time in its environment the spatial scale of the grid pattern contracts, and the 'gridness', a measure of symmetry, gradually increases. We study this phenomenon using biophysically realistic neuronal networks. The neurons in our network are conductance-based neurons modeled as layer II stellate cells that are coupled via inhibitory interneurons. Previous experiments in brain slices have discovered Spike timing dependent plasticity (STDP) in the Inhibitory synapses of the mEC, which could potentially reshape the topology of grid cell networks present in this region. In our study, we demonstrate that changes in the topology of the neuronal network, brought about by STDP, in conjunction with the modulation of the theta rhythm from the medial septum can replicate the dynamics observed in the mEC as the animal becomes progressively familiar with its environment.

Contents

1	Introduction	5
1.1	The Hippocampal cognitive map	5
1.2	Neuronal Plasticity in the Hippocampus	6
1.3	Our work: Using Stellate cell circuits to study network-level learning . .	8
2	Materials and Methods	10
2.1	Neurons	10
2.2	Synapses	12
2.3	Neuronal network architecture	13
2.4	A biologically plausible learning rule - STDP	17
2.5	Data Analysis	19
3	Results	21
3.1	Modelling iSTDP at the synapse	21
3.2	Inhibitory STDP gives rise to an asymmetry in network weights	24
3.3	Learning causes a shift of the robust regime in frequency space	27
3.4	Asymmetry in the network connectivity reduces the width of neuronal bursts and defines a direction of propagation	31
4	Discussions	35
4.1	Network connectivity - Experiments, Results and Inferences	35
4.2	Extending our study to 2D trajectories	37
4.3	Similarities with hippocampal sequences and memory consolidation . .	39
5	Appendices	42
5.1	Neuronal parameters	42
5.2	Synaptic parameters	46
5.3	STDP parameters	47

List of Figures

1	Grid cell response to novelty - panel adapted from Barry, Ginzberg, et al. 2012	8
2	The two states in our synapse model	14
3	Schematic - Grid fields of four neurons	15
4	Mapping a straight line trajectory to a ring of neurons	15
5	Neuronal network architecture	16
6	Schematic showing the behavior of the STDP equations	19
7	Inhibitory STDP in the mEC - panel adapted from Haas, Nowotny, and Abarbanel 2006	22
8	The STDP curve obtained by simulation	23
9	Connectivity kernels - before and after STDP	25
10	Changes brought about by STDP in the network	26
11	The shift in the robust regime brought about by STDP	28
12	Snapshots of different squares in figure 11	29
13	Theta frequency decreases in novel environments - figure adapted from Jeewajee et al. 2008	30
14	Asymmetry decreases inter-burst intervals and burst widths	32
15	Propagation of sequences with an external input	33
16	Two possible types of connectivity kernels	36
17	Extending our model to two dimensions	38
18	Propagation of sequences in an asymmetric network with no external input	40
19	IE and EI connectivity kernels	46

1 Introduction

The Hippocampus and associated regions, commonly referred to as the Hippocampal formation, are some of the most well studied and characterized regions of the brain, at the level of both, individual neurons and circuits. Electrophysiological experiments, lesion studies and insights gathered from patients lacking these regions have led to the understanding that these regions play important roles in the formation of memories, and spatial navigation. In the succeeding introduction, I will briefly talk about what we currently know about spatial navigation and hippocampal plasticity, and explain the phenomenon we have tried to model during my Master's thesis.

1.1 The Hippocampal cognitive map

Studying the behavior of rats in artificial mazes, Edward Tolman put forth the hypothesis that animals form an internal representation (commonly called map) of the environment, and use this representation to perform tasks such as navigation and reward procurement (Tolman 1948). Tolman coined the term 'cognitive map' for internal representations of this sort, and they have subsequently been accordingly referred. Tolman, however, was unable to provide any conclusive experimental evidence to prove that animals indeed build such representations.

In 1971, while recording the activity of neurons in the hippocampus, Dostrovsky and O'Keefe found that certain neurons increase their firing rate drastically whenever the animal occupies certain locations in space (O'Keefe and Dostrovsky 1971). This selective preference to certain places in the environment earned these cells the name, 'place cells'. Place cells showed a number of interesting properties, perhaps two of the most striking ones among these were **a.** place cells change their receptive field if landmarks present in the environment are rotated/moved, the change in the position of the receptive field mimicing the change in the position of the landmark and **b.** small changes in the environment are represented by modulating the firing rates of the existing place cell ensemble coding for the room (rate remapping), whereas larger changes are represented by a complete change in the place cell ensemble representing the environment (global remapping). The dependence on landmarks shows that animals store previous maps of the environment in the brain, and accordingly modify this map when there is a change to the environment. However, when a large change is made, the animal represents this change with a completely different set of cells. These two observations completely agree with the 'cognitive map' theory (O'Keefe and Dostrovsky 1971).

Ever since this seminal discovery, a number of other cells have been identified that are sensitive to various parameters of the animal-environment interactive system. In this menagerie of cell-types, two discoveries have been of paramount importance in changing the way we perceive spatial navigation, these are head-direction cells and grid cells (E.I. Moser, M.-B. Moser, and McNaughton 2017). Head-direction cells, as the name suggests, are cells that respond when the animal is facing a particular direction (Taube, Muller, and Ranck 1990, Taube, Muller, and Ranck 1990). Initially identified in the dorsal presubiculum, these cells have subsequently been found across cortical and subcortical regions (E.I. Moser, M.-B. Moser, and McNaughton 2017). The existence of head-direction cells is indicative of the fact that the hippocampus might be integrating head angular velocity to calculate heading direction. Heading direction coupled with velocity of motion (obtained from various sensory modalities) could be used to calculate the instantaneous location of the animal. This was one of the first discoveries hinting at the use of idiothetic reference frames (the position of the animal is specified with respect to an arbitrary reference point) for spatial navigation. Navigation in such a reference frame, i.e. calculating position via integration of self-motion cues, is known as path-integration. The discovery of head-direction cells directly point towards the existence of a path-integration system in an idiothetic reference frame (E.I. Moser, M.-B. Moser, and McNaughton 2017).

The identification of this wide assortment of cells that respond to different features of the environment, had bolstered the notion of the existence of the hippocampal cognitive map, the discovery of Grid cells in the Entorhinal Cortex rendered this idea nearly indubitable (E.I. Moser, Roudi, et al. 2014, E.I. Moser, M.-B. Moser, and McNaughton 2017). The properties of grid cells hinted at them being a possible neural substrate for path integration, and the animal's metric of space. Grid cells are neurons that fire action potentials whenever the animal is located at the vertices of a tessellating grid of equilateral triangles (Hafting et al. 2005). Unlike place fields, these spatially periodic, hexagonal receptive fields of grid cells are nearly universal, in that the same hexagonal repeating pattern (for a single cell) forms in almost all environments (Hafting et al. 2005). The robust grid pattern formed by these cells is nevertheless affected by a few factors, such as the geometry of the boundary of the environment, the novelty/familiarity of the environment, presence of compartments in the environment etc (Barry, Ginzberg, et al. 2012, Barry, Hayman, et al. 2007, Krupic et al. 2015).

1.2 Neuronal Plasticity in the Hippocampus

The Hippocampus has also been a prolific area for the study of synapses and their maturation over time. The study of synapses in this region viz. Hippocampal synapses, has

helped neuroscientists gain fundamental insights on how the brain learns and adapts to its environment. It has been postulated, and verified in many cases that the brain encodes information (learning) and memories through changes in the efficacy of the presynaptic neuron, as one of the neurons that activate a postsynaptic neuron. One could say that changes in synaptic strength encode learning and memory (T.V. Bliss and Collingridge 1993, Martin, Grimwood, and Morris 2000).

Many of these ideas were conceived and formulated through the study of hippocampal synapses. Historically, these studies were performed by providing patterned activation to certain subsets of neurons, either presynaptic, or both presynaptic and postsynaptic. Following this patterned input, the changes in synaptic efficacy as a function of the patterned activation, was noted. Such studies led to the identification of two forms of plasticity that have different timescales for the change in synaptic efficacy, aptly named as short term potentiation (STP) and long term potentiation (LTP) (Martin, Grimwood, and Morris 2000). A detailed study of the processes that underlie synaptic transmission allowed researchers to understand some of the salient factors that determine the type of plasticity, e.g. STP is predominantly determined by presynaptic calcium stores, whereas LTP is enabled by the NMDA receptor (T.V.P. Bliss and Lømo 1973, T.V. Bliss and Collingridge 1993, Martin, Grimwood, and Morris 2000).

Numerous studies have found that the change in synaptic strength depended upon the order and time difference between presynaptic and postsynaptic activation. This form of asymmetric Hebbian learning has been called Spike-timing dependent plasticity (STDP). STDP, a type of synaptic learning rule has been found to exist in multiple regions of the brain (Markram et al. 1997, Bi and Poo 1998). Different types of STDP - excitatory and inhibitory, with different learning curves have been documented (Markram et al. 1997, Bi and Poo 1998, Haas, Nowotny, and Abarbanel 2006, Vogels et al. 2013).

While these studies have been very useful in understanding the molecular and cellular level changes that underlie learning, it has not been possible to understand how learning is represented at the level of the network. In other words, we do not know what differentiates a network that has 'learned' from other neuronal networks. The study of Grid cell networks in the Entorhinal Cortex provides the ideal system for approaching this question.

1.3 Our work: Using Stellate cell circuits to study network-level learning

When an animal is introduced to a novel environment, the hexagonal symmetry of the grid pattern gets distorted, the size of individual receptive fields and the spacing between neighbouring receptive fields increases. As the animal gets familiarized with its environs, the hexagonal symmetry of the pattern gets gradually restored, and the diameter and spacing of individual grid cell receptive fields attain steady values (Barry, Hayman, et al. 2007, Barry, Ginzberg, et al. 2012). The mechanisms and changes in the Entorhinal Cortex underlying this internal shift in the state of the animal, as the familiarity with its environment increases, remain largely unknown.

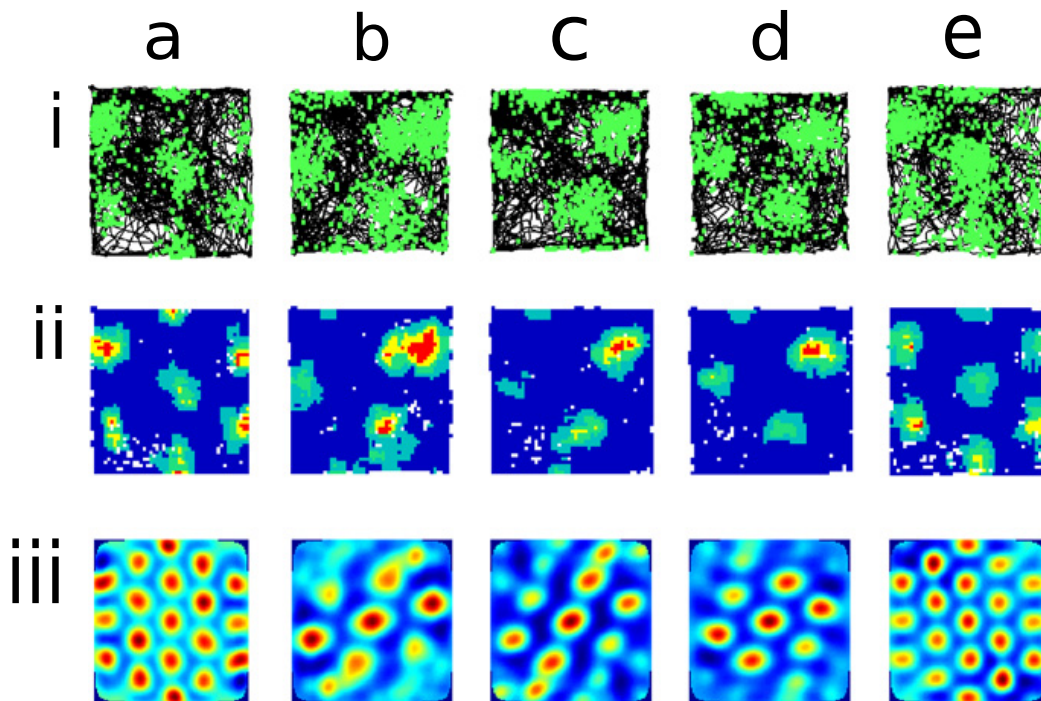


Figure 1. A figure panel adapted from Barry, Ginzberg, et al. 2012 showing changes in grid fields brought about by different environments. Column **a** and **e** were trials conducted in familiar environments, columns **b-d** were trials conducted in environments novel to the animal. The first row (**i**) shows the trajectory of the animal (black) and locations where the grid cell was active (light green). The middle row (**ii**) is a firing rate map (**red**-high firing, **blue**-low firing and **white**-unvisited locations). The last row (**iii**) is a spatial-autocorrelogram. For details on the exact values of peak firing rate, 'gridness' of the pattern and how the spatial autocorrelogram was constructed, the reader can consult Barry, Ginzberg, et al. 2012.

Stellate cells are cells found in the medial Entorhinal Cortex (mEC) that are thought to be grid cells. We propose a novel idea, the use of Stellate cell circuits to study

the changes that learning brings about networks. The emergence of spatially periodic, repeating receptive fields is believed to be a property of Stellate cell networks. Such receptive fields have been obtained through a variety of computational models that employ different principles (Fransén et al. 2004, Burak and Fiete 2009, Hasselmo and Shay 2014, O'Keefe and Burgess 2005, Giocomo, M.B. Moser, and E.I. Moser 2011). The composition, architecture and nature of inputs to the Stellate cell network wholly decide the activity of each of the individual neurons that comprise the network. Given that there are visible change in the receptive fields of a neuron as the animal learns the environment, and since changes in individual receptive fields of cells are believed to be a network property, it is only natural that changes to stellate cell networks, brought about by the learning, cause these changes.

Previous electrophysiological experiments in Layer II/III of the mEC have established the existence of Inhibitory Spike-timing dependent plasticity (iSTDP) at the synapses between the Inhibitory interneurons and Stellate cells (*IE* synapses) (Haas, Nowotny, and Abarbanel 2006). In this study, we attempt to study the changes that iSTDP brings about in a network, as the animal becomes progressively familiar with its environment. Given that there are no Excitatory-Excitatory synapses (*EE* synapses) in the mEC, and Inhibitory interneurons are the primary inputs to Stellate cells in this region (Couey et al. 2013, Schmidt et al. 2017), we hypothesize that the changes in the firing patterns of Stellate cell networks are brought about by inhibitory plasticity.

For my Master's thesis, we address this problem by modeling neuronal networks comprising biophysically realistic neurons and synapses. The *IE* synapses of the network are plastic, and the efficacy of the synapse evolves in accordance with experimentally characterized plasticity rules (Haas, Nowotny, and Abarbanel 2006). All our simulations, and parameter values have been based on insights and evidences from experiments. The following sections of this thesis will detail the relevant experiments, and our attempts to model this extremely interesting transformation in the spatial scale of grid cell patterns.

2 Materials and Methods

All simulations were performed using C++ and *insilico*, a C++ library developed at the Computational Neuroscience Lab, IISER Pune (<http://www.iiserpune.ac.in/collins/insilico/>). The development of *insilico* was motivated by the desire to allow the programmer to focus on details pertaining to the simulation, without spending too much time on the actual coding and debugging aspects. *Insilico* uses odeint - a C++ library developed for solving the Initial value problems of Ordinary differential equations by iterative numerical integration (Ahnert and Mulansky 2011). All simulated data was obtained in the form of .dat files, whose analysis was carried out using python 2.7.6 and various other python libraries.

2.1 Neurons

We have modelled both Stellate cells and Inhibitory neurons as biophysically realistic point entities. In some parts of this thesis, we will be using the abbreviation E neurons for Stellate cells/Excitatory neurons, and I neurons for Inhibitory interneurons. The Stellate cell model has been based on a previous model of a Layer II/III stellate cell in the medial Entorhinal Cortex(mEC) (Rotstein et al. 2006). This model is an extension of the Hodgkin-Huxley model of the neuron. In addition to the standard sodium (I_{Na}), potassium (I_K) and leak channels (I_L), this neuron has a persistent sodium channel (I_{NaP}), and a two component (fast and slow) hyperpolarization-activated current (I_h). Stellate cells in the medial Entorhinal Cortex have been shown to exhibit low-amplitude (1-4 mV) oscillations at theta-rhythm frequencies, commonly referred to as subthreshold oscillations (STOs). Previous studies show that the interplay between the persistent sodium current and the hyperpolarization-activated current is sufficient to explain the emergence of STOs (Dickson et al. 2000, Fransén et al. 2004). Stellate cells have been shown to exhibit characteristic rebound spikes after inhibition from interneurons. Computational models that include the I_h current, and pharmacological experiments that block HCN channels (responsible for the I_h current) have established that the I_h current is necessary for the production of these rebound spikes after receiving inhibition (Dickson et al. 2000).

The current equation for this model of a Stellate cell is below:

$$C \frac{dV}{dt} = I_{ext} + I_{DC} - I_{Na} - I_K - I_L - I_h - I_{NaP} - I_{syn} - I_{Noise} \quad (1)$$

where V is the membrane potential (mV), C is the membrane capacitance ($\mu F/cm^2$),

I_{ext} is an externally applied bias to the neuron ($\mu A/cm^2$), I_{DC} is the applied DC to the neuron that stays constant throughout the simulation, I_{syn} is the current that flows into the neuron through the synapse and I_{Noise} is a noise term introduced in the synaptic current. I_{osc} is any form of oscillating current that is given to the neuron. For the Entorhinal Cortex circuit that we are modelling, we use this oscillating current to simulate the theta rhythm input from the medial septum (MS). The channel currents are defined by the following differential equations:

$$\begin{aligned}
I_{Na} &= G_{Na}m^3h(V - E_{Na}) \\
I_K &= G_Kn^4(V - E_K) \\
I_L &= G_L(V - E_L) \\
I_{NaP} &= G_pp(V - E_{Na}) \\
I_h &= G_h(0.65r_f + 0.35r_s)(V - E_h)
\end{aligned} \tag{2}$$

G_X and E_X ($X = Na, K, L, p, h$) are the maximal conductances (mS/cm^2) and reversal potentials (mV) respectively. The units of time are $msec$. All the gating variables x (where $x = m, h, n, p, r_f, r_s$) obey first order differential equations of the form:

$$\frac{dx}{dt} = \frac{x_\infty(V) - x}{\tau_x(V)}, \tag{3}$$

where

$$x_\infty(V) = \frac{\alpha_x(V)}{\alpha_x(V) + \beta_x(V)} \quad \text{and} \quad \tau_x(V) = \frac{1}{\alpha_x(V) + \beta_x(V)} \tag{4}$$

The voltage dependent parameters $\alpha_x(V)$ and $\beta_x(V)$ have been defined as functions that show some form of exponential dependence on x . Due to space constraints, we haven't specified the functions of $\alpha_x(V)$ and $\beta_x(V)$ in this section. For the exact functional forms of $\alpha_x(V)$ and $\beta_x(V)$, where $x = m, h, n, p, r_f, r_s$, the interested reader can consult section 5.1.

The inhibitory neuron model we have used is based off the Inhibitory neurons modelled in the work by Wang and Buzsaki (Xiao-Jing Wang and György Buzsáki 1996). The current equation for this model of the inhibitory neuron is given below:

$$C \frac{dV}{dt} = I_{ext} + I_{DC} - I_{Na} - I_K - I_L - I_{syn} - I_{osc} - I_{Noise} \tag{5}$$

The sodium (I_{Na}), potassium (I_K) and leak (I_L) currents have been modeled according to Hodgkin and Huxley's equations, written in equation 2. However, the maximum conductance values and gating variables have been modified to make the inhibitory interneurons show characteristic behaviors of hippocampal and neocortical interneurons. These interneurons exhibit a brief after-hyperpolarization phase of -15 mV , which transiently takes the membrane potential to values around -70 mV , this has been implemented by setting the maximum value of potassium conductance (G_K) to low values, and a fast gating variable for I_K so as to ensure that it deactivates quickly during the spike repolarization. Another striking property of these interneurons is their ability to generate fast, repetitive spikes, this has been implemented by having fast kinetics for sodium inactivation (h) and potassium activation (n), and a relatively high threshold for the potassium current, I_K (Xiao-Jing Wang and György Buzsáki 1996). A list of all the variables and the values assigned to them in the simulations, can be found in Xiao-Jing Wang and György Buzsáki 1996. A description of the synaptic current, I_{syn} , and details on how it's computed can be found in section 2.2 and equation 8.

2.2 Synapses

Our network consists of two types of neurotransmitter-receptor pairs, AMPA for Excitatory-Inhibitory synapses (EI synapses) and GABA_A for Inhibitory-Inhibitory synapses (II synapses) and Inhibitory-Excitatory synapses (IE synapses). Since Stellate cells have been found to connect to other Stellate cells only via inhibitory interneurons (Couey et al. 2013), we do not include EE synapses in our network.

All conductances (AMPA and GABA_A) in the network have been modelled as simple first-order kinetic reactions. Each postsynaptic receptor is assumed to exist in any one of two configurations, open or closed. The probability of the receptor remaining in the closed state is $1 - P_r$, whereas the probability of remaining in the open state is P_r . In the simulation, these probabilities are a function of time, and depend on the presence/absence of neurotransmitter in the synaptic cleft. α is the rate at which each channel switches from closed to open state, and β is the rate at which the channel switches from open to closed state. This can be represented in the differential equation:

$$\frac{dP_r}{dt} = \alpha(1 - P_r) - \beta P_r \quad (6)$$

For simplicity, we model the neurotransmitter in the synaptic cleft as a square pulse [Figure 2]. The neurotransmitter concentration in the synaptic cleft rises sharply after

the arrival of a presynaptic action potential. In the simulation environment, this instant of time is defined as the "last spike" of the presynaptic neuron (t_{n-1}). The concentration of neurotransmitter in the synaptic cleft drops down to zero after a fixed duration of time (T_d). This approximation ensures that the neurotransmitter concentration in the synaptic cleft takes binary values, allowing us to simplify calculations by specifying α and β values for each of the two states of the synapse.

State 1 - $\beta \sim 0$, lasts for a duration of T_d after the presynaptic neurons fires

State 2 - $\alpha \sim 0$, for all other values of time in the simulation

After reducing the complexity of our synapse, the modified time differential equation for probability depends only on the state of the synapse, as shown in equation 7 and figure 2. The probability of a channel remaining open, is calculated by numerical integration of the following differential equation:

$$\frac{dP_r}{dt} = \begin{cases} \alpha(1 - P_r) & \text{for } t'_{n-1} \leq t \leq t'_{n-1} + T_d \\ -\beta P_r & \text{for other values of } t \end{cases} \quad (7)$$

The value of the postsynaptic conductance in mS/cm^2 is specified as a product of the maximum value of conductance and the probability of a channel being in the open state. This can be intuitively thought of as the fraction of receptors on the postsynaptic density that remain in the open state. Each postsynaptic conductance directly feeds into the postsynaptic neuron in the form of a postsynaptic current (I_{syn}) mentioned in equation 2, which is given by the product of the postsynaptic conductance and difference between the membrane potential and resting potential [Equation 8].

$$I_{syn} = G_{syn} P_r (V - E_{syn}) \quad (8)$$

2.3 Neuronal network architecture

The overall architecture of the network resembles that of continuous attractor models that have been used to explain grid cell firing (Burak and Fiete 2009, Giocomo, M.B. Moser, and E.I. Moser 2011). However, certain differences between our model and other models allow us to effectively study the motion of an animal in one dimension. These features of the model have been described below.

An individual grid cell's receptive field tessellates space. Figure 3 shows the receptive fields of adjacent grid cells, superimposed. Looking at this schematic, it becomes ev-

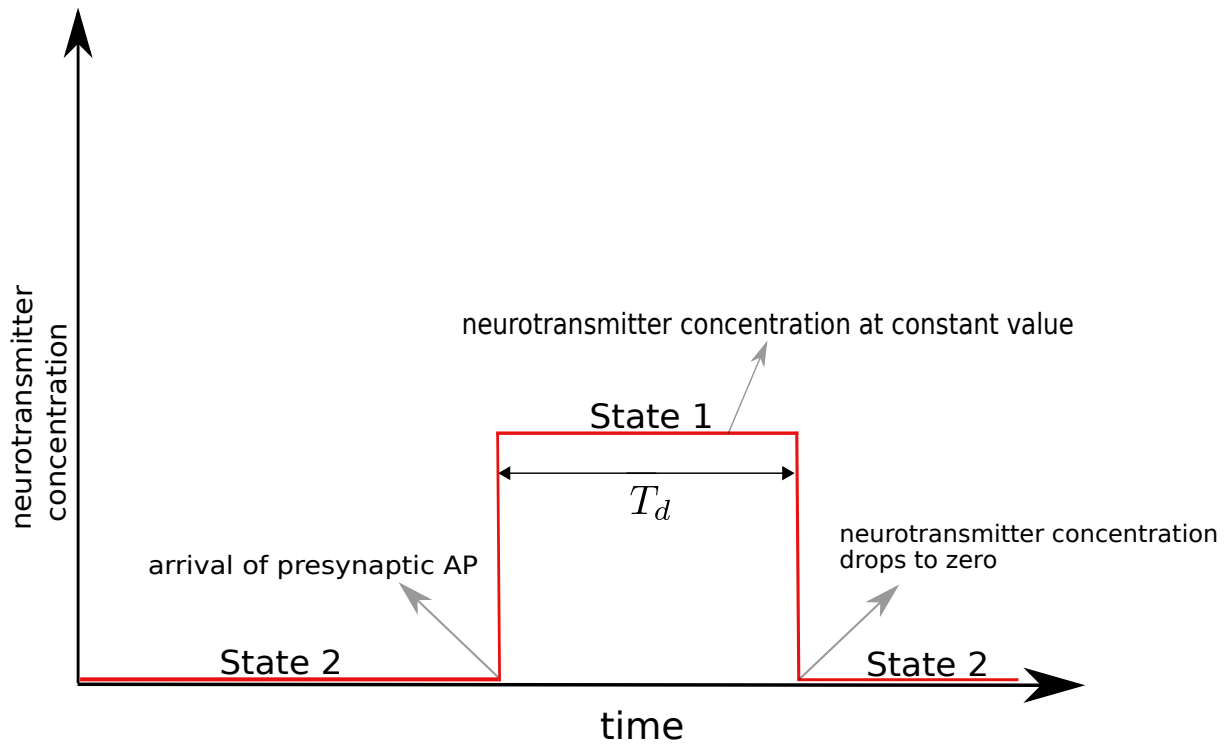


Figure 2. A schematic showing the two states in our synapse model and how the neurotransmitter concentration in the synaptic cleft varies depending on the state of the synapse. Section 2.2 describes the reasons for modelling the synapse in such a manner.

ident that as the animal travels through space, the trajectory of the animal is mapped onto the activity of a sequence of grid cells. If one considers linear trajectories through space (shown by white lines in figure 3), the animal's path will be encoded by a set of periodic, repeating receptive fields, as shown in figure 4.

Thus, every linear trajectory in space can be mapped onto the repetitive, periodic activity of a group of cells. One can think of this periodic activity as the successive activation of neurons in a ring. This was the primary reason for us to construct our network in the form of two concentric rings. This simplistic transformation from linear trajectories to ring networks, shown in figure 4 prompted us to start our investigation by analyzing linear trajectories.

Our model has two rings, a ring of I neurons, and a ring of E neurons. To make it easy to visualize this network, one can imagine two concentric rings, an inner ring of I neurons and an outer ring of E neurons. A striking feature of our model is that the inner ring of I neurons that are all-all connected. This type of connectivity is a standard recipe for a winner-takes-all paradigm, and forces the peak of activity to stay at one interneuron at a time (Assisi, Stopfer, and Bazhenov 2011). After an inhibitory

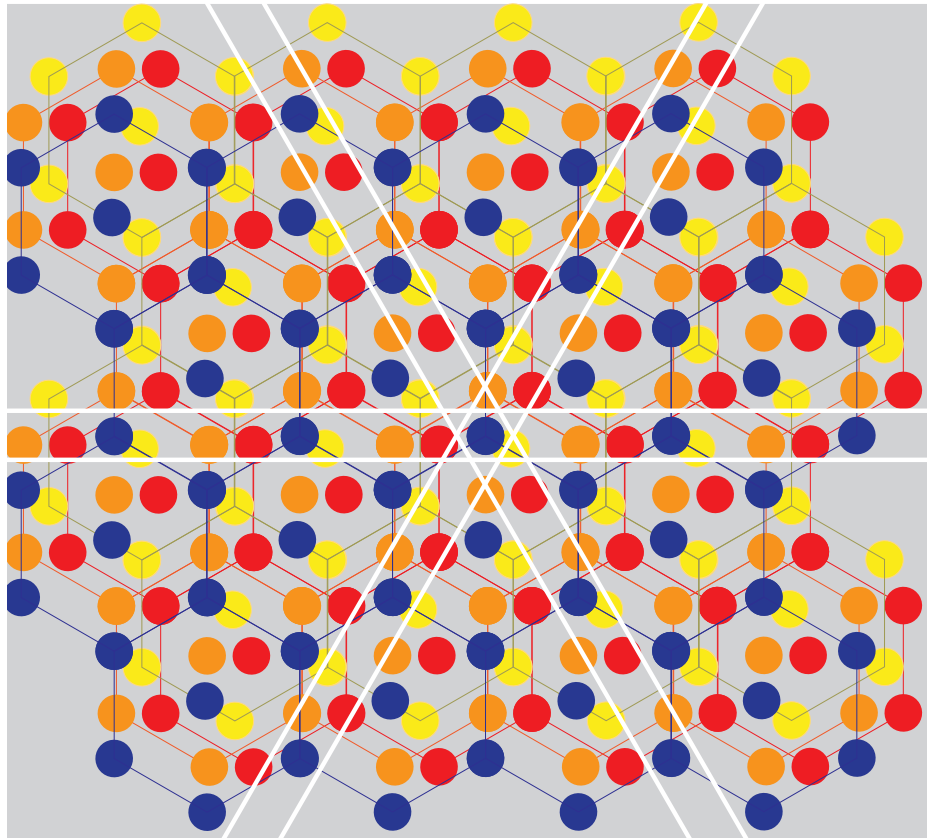


Figure 3. A schematic showing all the grid fields of four different neurons (marked in red, blue, orange and yellow) in a particular environment. The three pairs of white parallel lines indicate three possible straight line trajectories of the animal.

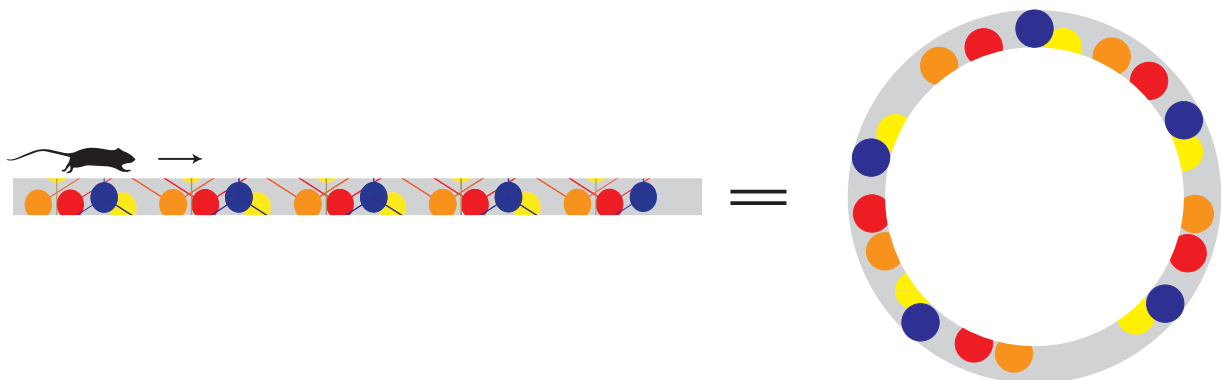


Figure 4. The straight line trajectory that the rat travels has been taken from the horizontal pair of white parallel lines in figure 3. As the rat travels along this path, the sequence of grid cells activated will be periodic and repeating. This sequential activity can be mapped onto the periodic activity of neurons on a ring.

neuron fires, it activates the nearest excitatory neuron via rebound after inhibition, as explained in section 2.1. Thus, the activity of excitatory neurons, in our network, is a faithful representation of the activity of inhibitory interneurons.

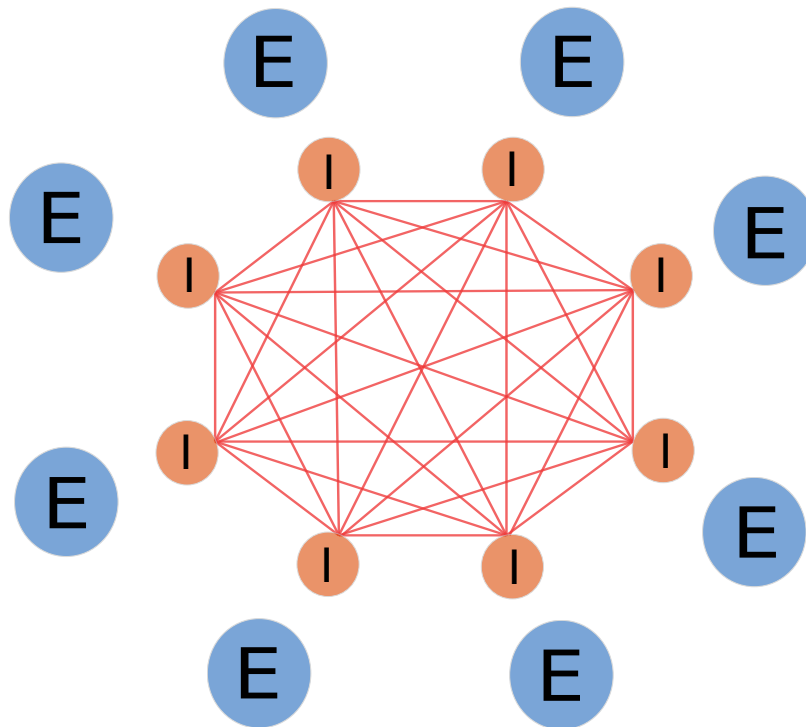


Figure 5. A schematic showing the architecture of our neuronal network. Blue circles - Excitatory neurons (Stellate cells), orange circles - Inhibitory interneurons. The red lines indicate the all-all inhibitory network of the interneurons. For the purposes of clarity, we haven't drawn the IE and EI synapses. Figure 9 shows the IE and EI connectivity kernels in detail, before and after STDP.

In all our network simulations (except one simulation in section 3.4), we have included an external input that is provided to inhibitory interneurons. This 'external input' is a constant DC current that is given to one neuron at a time in the network, and shifts between neurons in a cyclic manner with the specified frequency (ε = frequency with which the external drive shifts between neurons on the ring). Since we started off with completely symmetric network weights in our simulation, it was imperative to have an extraneous determinant of activity propagation direction. The external input given to a neuron played this role, ensuring that the activity bump preferentially flowed from one I neuron to the adjacent I neuron. While there isn't any experimental evidence that the connectivity of inhibitory neurons in a given volume of the mEC resembles that of a complete graph, this assumption allows us to mimic a winner-takes-all scenario where the activity shifts between neurons.

Each inhibitory neuron is connected to excitatory neurons in the other ring in such a way that neurons that are closer to each other have a greater value of synaptic weight. This form of local connectivity has been implemented by modelling the outgoing synap-

tic weight profile of each neuron as a Gaussian. The EI connectivity profile has been defined slightly differently, instead of a single-peaked Gaussian, the EI connectivity profile comprises two peaks which are slightly shifted away from the E neuron, in opposite sides of the ring. Figure 5 is a schematic that shows some features of the network architecture. A figure detailing the exact IE and EI connectivity kernels used in our simulations can be found in panel **a** of figure 9. Our justification for including such an external input in our simulations, modelling the EI and IE connectivity kernels in such a manner, and other discussions can be found in section 3.2.

2.4 A biologically plausible learning rule - STDP

Spike-timing dependent plasticity (STDP) is a type of asymmetric Hebbian learning rule. Initially characterized in excitatory cortical and hippocampal synapses, STDP has subsequently been identified in many other brain regions and is thought to underlie processes like Long-term potentiation (LTP) and Long-term depression (LTD), which are potential candidates for memory formation and forgetting (Markram et al. 1997, Bi and Poo 1998, T.V. Bliss and Collingridge 1993). Inhibitory STDP (iSTDP) is a type of STDP where the presynaptic neuronal activity hyperpolarizes the postsynaptic neuron. With repeated pairings of presynaptic neuron (pre) and postsynaptic activity (post), inhibitory STDP causes an increase/decrease in the strength of inhibition. The change in slope of the Inhibitory postsynaptic potential (IPSP), or the peak value of the IPSP can be used as a proxy for the strength of inhibition on the postsynaptic neuron (Haas, Nowotny, and Abarbanel 2006, Vogels et al. 2013).

We have used an online implementation of STDP to model the rules that underlie weight learning at the synapse (Morrison, Diesmann, and Gerstner 2008). A detailed account of the experimental demonstration of Inhibitory STDP, and our reason for choosing to model this phenomenon using a differential equation model can be found in section 3.1. This model of STDP assumes two hypothetical variables, x - linked with the presynaptic neuron and y - linked with the postsynaptic neuron. Each time the presynaptic neuron spikes, there is a jump in the value of x (implemented through a δ function). Barring this jump caused whenever the neuron spikes, the value of x obeys an exponential decay with a specific time constant. Variable y exhibits a similar behavior with respect to the postsynaptic neuron [Figure 6]. a_+ and a_- are constants that determine the height of jump caused in variables x and y respectively. The time-dependence of these equations has been expressed in the differential equations below.

$$\begin{aligned}
\tau_+ \frac{dx}{dt} &= -x + a_+(x) \sum_i \delta(t - t_i - t_{xlag}) \\
\tau_- \frac{dy}{dt} &= -y + a_-(y) \sum_j \delta(t - t_j - t_{ylag})
\end{aligned} \tag{9}$$

Where t_i and t_j for $i, j = 1, 2, 3 \dots$ denotes the firing times for the presynaptic and postsynaptic neurons respectively, and t_{xlag} and t_{ylag} are respective lag times for the onset of x and y variables [See figure 6]. For every iteration, the values t_{xlag} and t_{ylag} are drawn from a Gaussian distribution of mean = 8.0 msec and variance = 1.0 msec².

For a biophysical understanding of the molecular players governing the variance in synaptic weight, one can liken x to the amount of glutamate bound to receptors on the postsynaptic density (PSD) or the fraction of NMDA receptors existing in the open state. Similarly, one can think of y as the voltage at the synapse caused by the backpropagating action potential, or the calcium entry due to the backpropagating action potential.

The change in synaptic weight is specified using these x and y variables. Each time the postsynaptic neuron spikes, the weight of the synapse is increased by a value proportional to the value left by trace y , and each time the presynaptic neuron spikes the value of the synapse is decreased by a value proportional to the trace x at that instant. This update rule is written in the form of the differential equation below.

$$\frac{dw}{dt} = A_+(w)x(t) \sum_j \delta(t - t_j) - A_-(w)y(t) \sum_i \delta(t - t_i) \tag{10}$$

The terms $A_+(w)$ and $A_-(w)$ are functions that act as weighting factors in equation 10. It makes sense, biologically, to keep the weight of the synapse in a fixed range. We can use the terms $A_+(w)$ and $A_-(w)$ to ensure that the weight of the synapse stays within the fixed range. We have accomplished this by setting $A_+(w)$ and $A_-(w)$ as functions with a multiplicative weight dependence, called soft bounds, defined in equation 11.

$$\begin{aligned}
A_+(w) &= (w_{max} - w)\eta_+ \\
A_-(w) &= w\eta_-
\end{aligned} \tag{11}$$

Where η_+ and η_- are positive constants and w_{max} is the maximum possible weight of the synapse. This values of $A_+(w)$ and $A_-(w)$ ensures that the weight of the synapse

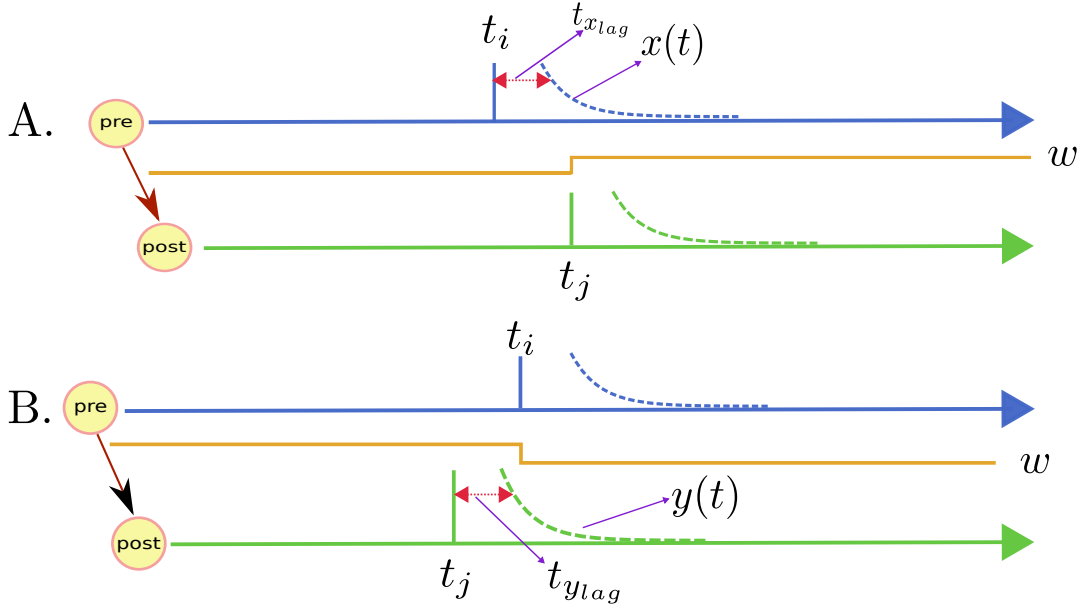


Figure 6. A schematic showing how the differential equations 9 and 10 behave. Panels **A.** and **B.** show cases where $t_{post} - t_{pre} > 0$ and $t_{post} - t_{pre} < 0$ respectively. The blue and green lines show the behavior of the presynaptic and postsynaptic neurons in time, respectively. The behavior of x and y variables have been depicted as blue and green dashed lines, respectively. The synaptic weight (w), which depends on the instantaneous values of x and y , has been marked in yellow ochre. One can see that whenever $t_{post} - t_{pre} > 0$ the weight of the synapse increases, and whenever $t_{post} - t_{pre} < 0$ the weight of the synapse decreases. This prediction is in accordance with the experimental STDP curve obtained by Haas, Nowotny, and Abarbanel 2006, shown in figure 7.

remains between 0 and w_{max} . The advantage of using an online model of this form is that it becomes possible to account for the contribution of every spike generated by every neuron in the entire network, to the weight of a particular synapse. While this may be computationally very intensive to simulate, I believe that this level of detail is imperative, especially when one is studying synaptic phenomena such as learning with the help of biophysically detailed models.

2.5 Data Analysis

All simulated data was generated in the form of text files (.dat files). The analysis of these files was carried out in Python 2.7.6. Most of the analysis code was developed over the course of the project and extensively used the *numpy* and *scipy* Python libraries. To calculate the parameters like the inter-burst interval, burst widths and robustness of the firing sequence, we did the following:

Firstly, we represented the entire network activity in the form of spike rasters. To do this, we used the peak-detector function available openly at <https://github.com/demotu/BMC> (author: Marcos Duarte). After converting the entire dataset to spike timepoints, we calculated inter-spike intervals (ISI) by looking at the time difference between spikes. To differentiate a spike occurring as a part of a burst from a stray spike, we set a threshold of 1700 *msec*, i.e. if the ISI is greater than 1700 *msec* then then the two spikes would not be a part of the same burst. After segregating all the spikes into bursts and stray spikes, it was possible to calculate parameters like the inter-burst interval and burst width.

Now, in order to define a robustness measure for the data presented in section 3.3, we compared the spike rasters for the 10 different trials of the network. This was done to check the pairwise-similarity between all of the trials. As a measure of similarity between trials, we used a discrete measure of spike synchronization defined by Mulansky and Kreuz 2016. The libraries defined by Mulansky and Kreuz 2016 are available in the python library, pypike. The SPIKE-Synchronization measure is defined as an normalized coincidence detector, where the coincidence window is an adaptive function of the ISI for the neurons being compared (equation 12). The ISI for neuron m at the i^{th} spike (ν_i^m) is defined as $\nu_i^m = t_{i+1}^m - t_i^m$, where t_{i+1}^m and t_i^m are the $i + 1^{th}$ and i^{th} spikes of neuron m , respectively.

$$\tau_{ij}^{m,n} = \frac{1}{2} \min(\nu_i^m, \nu_{i-1}^m, \nu_j^n, \nu_{j-1}^n) \quad (12)$$

where $\tau_{ij}^{m,n}$ is the adaptive coincidence defined for the i^{th} and j^{th} spikes of neurons m, n respectively. After defining the adaptive window, the coincidence indicator for neuron m is defined by:

$$C_i^m = \begin{cases} 1 & \text{if } \min_j (|t_i^m - t_j^n|) < \tau_{ij}^{m,n} \\ 0 & \text{otherwise} \end{cases} \quad (13)$$

Now, in a similar fashion, one can define C_i^l , where $l = 1, 2, 3 \dots S$ is the total number of spike trains for which we are calculating the SPIKE-Synchronization measure. The value of synchronization (*SYNC*) for the series of spike trains can then be defined as:

$$SYNC = \frac{1}{S} \sum_{l=1}^S C_l = \frac{C}{M} \quad (14)$$

3 Results

3.1 Modelling iSTDP at the synapse

In 2006, while studying the electrophysiological properties of neuronal circuits in Layer II/III of the medial Entorhinal Cortex, (Haas, Nowotny, and Abarbanel 2006) found that the *IE* synapses in this region exhibit Inhibitory Spike-timing dependent plasticity (iSTDP). Stellate cells were identified by their characteristic electrophysiological responses to depolarizing and hyperpolarizing current injections, which were delivered through the patch clamp technique. Presynaptic Inhibitory neurons were activated via extracellular stimulation of 10 - 50 μA , within 100-200 μm of the recording patch clamped electrode. Presynaptic extracellular excitation was paired with postsynaptic activity (after a fixed duration in *msec*) by injecting currents of 1-3 *nA* through the recording electrode in current clamp mode. This pairing protocol was repeated for a duration of 3-5 *mins* at a frequency of 2 *Hz*. After this pairing protocol, the authors measured the ratio of the slope of the Stellate cell IPSP relative to the slope of the IPSP before the pairing protocol. This quantity has been used as a proxy for the potentiation of the *IE* synapse [Figure 7].

This pairing protocol was repeated for different values of time difference in postsynaptic (t_{post}) and presynaptic (t_{pre}) neuron firing, to obtain the STDP curve shown in figure 7. The STDP curve obtained was an asymmetric curve which potentiates for positive values of ($t_{post} - t_{pre}$), and depresses for negative values of the same. Both the peak values for potentiation and depression were obtained when the magnitude of time difference was found to be around ± 10 *msec*. However, the extents of potentiation and depression were found to be different.

Based on the best fit to the points on the STDP curve, the authors proposed a theoretical model to explain the function mapping ($t_{post} - t_{pre}$) values to changes in synaptic weights. This function is given below:

$$F(\Delta t) = \begin{cases} 1 + a_1(\Delta t)^{10}e^{a_2\Delta t}, & \text{for } \Delta t < 0 \\ 1 + a_3(\Delta t)^{10}e^{a_4\Delta t}, & \text{for } \Delta t > 0 \end{cases} \quad (15)$$

where $a_1 = -2.6 \cdot 10^{-7} ms^{-10}$, $a_2 = 0.94 ms^{-1}$, $a_3 = 2.29 \cdot 10^{-6} ms^{-10}$, $a_4 = -1.10 ms^{-1}$. While this function was able to explain the results of the STDP protocol used by the authors, it had a major drawback. The function could only account for a single pair of pre-post spikes, in other words, this was a memoryless function. However, in real

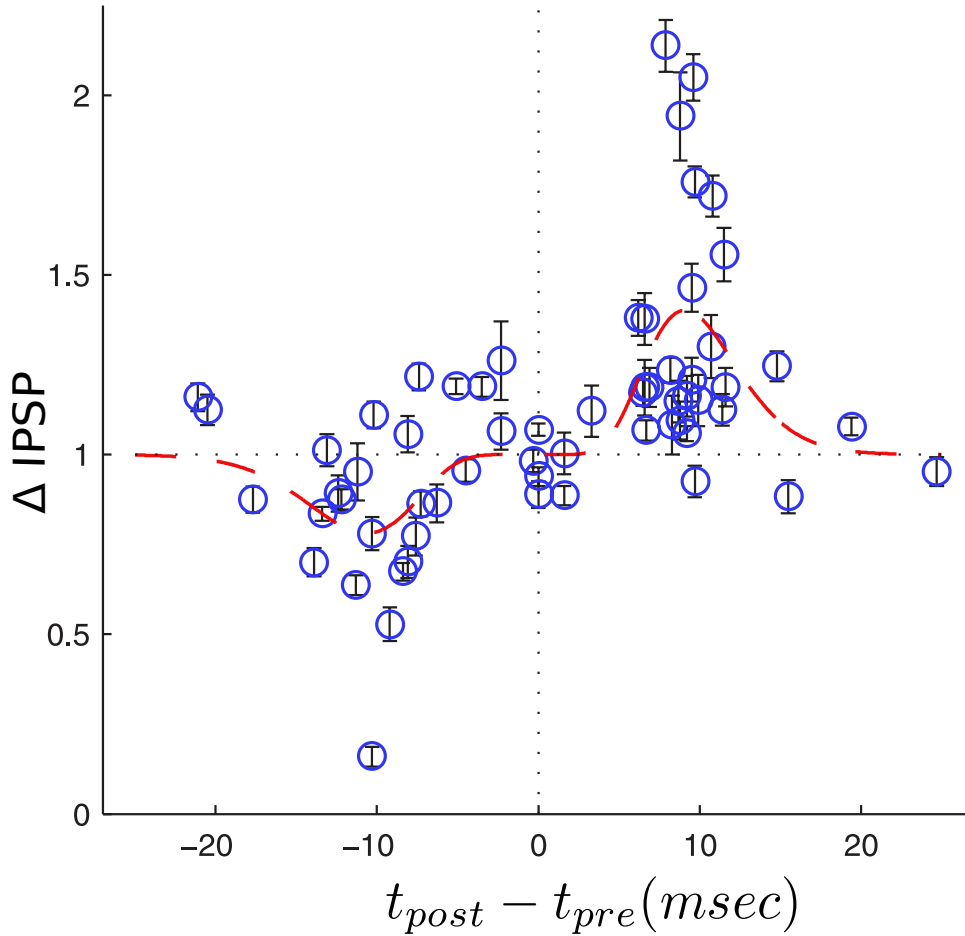


Figure 7. A figure panel adapted from Haas, Nowotny, and Abarbanel 2006 that shows the STDP curve for IE synapses in the mEC. The red dashed curve is the least-square error fit, that has been used to model equation 15. The y -axis (Δ IPSP) is the ratio of IPSP after the STDP protocol to the IPSP before the STDP protocol. The peaks of potentiation and depression lie at around ± 10 msec. The blue circles are individual data points obtained in the experiment, and the black error bars show the standard error for each of the points. For the exact details on the sample sizes and which data points showed a significant difference in Δ IPSP, the reader can consult Haas, Nowotny, and Abarbanel 2006.

biological systems, it has been found that the change in synaptic weights caused by pre-post pairings depends not only $t_{post} - t_{pre}$, but also depend on the firing rate, and cooperativity among inputs (Sjöström, Turrigiano, and Nelson 2001, Feldman 2012).

Given that the neurons in our model of an Entorhinal cortex circuit show bursting behavior, by using the model proposed in equation 15, we would miss out on most of the interesting detail and variability shown in our network model. More importantly, a model that doesn't take into account the effect of all spikes may not give us a realistic estimate of what really happens. Thus, in order to account for the effect of multiple

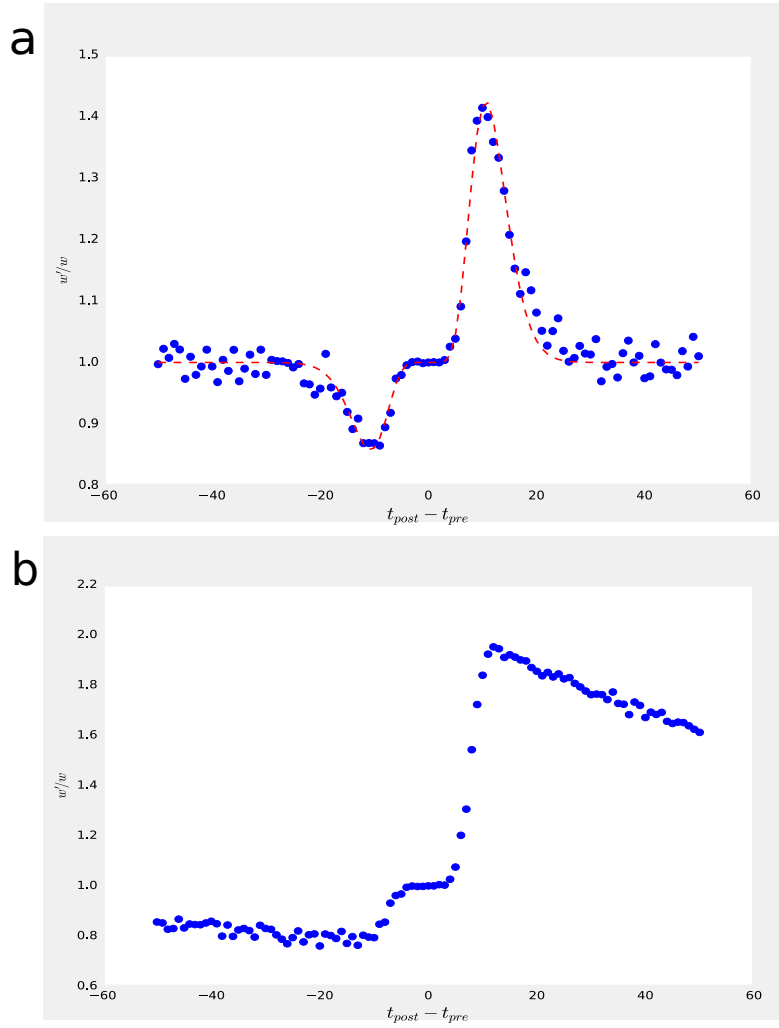


Figure 8. The STDP curves obtained by simulating the experimental protocol of Haas, Nowotny, and Abarbanel 2006. **a.** The STDP curve where $\tau_x = \tau_y = 5.0 \text{ msec}^{-1}$. The red dotted line is the least-square error fit of equation 15 for these data points. The values of the constants in equation 15 that gave produced the red-dotted line are $a_1 = -1.13 \cdot 10^{-7} \text{ ms}^{-10}$, $a_2 = 0.91 \text{ ms}^{-1}$, $a_3 = 4.36 \cdot 10^{-7} \text{ ms}^{-10}$, $a_4 = -0.93 \text{ ms}^{-1}$. **b.** The STDP curve where $\tau_x = \tau_y = 74.0 \text{ msec}^{-1}$.

presynaptic and postsynaptic spikes, we decided to use implement an online scheme for STDP, whose details have been presented in section 2.4.

The specifics of our STDP protocol were entirely based upon the Haas, Nowotny, and Abarbanel 2006 experiment, i.e. the number, frequency of pairings, intensity of applied current etc. were set to the same values that were used in the experiment. We found that a mere presentation of artificial spikes to the STDP differential equations 9 and 10 was almost identical to the STDP curve obtained by providing paired pulses to biophysically detailed point neurons. Thus, we performed our simulation of the STDP experiment by presenting artificially timed spikes to the STDP differential equations. The

number of free parameters that one could vary were $\tau_x, \tau_y, a_+(x), a_-(y), A_+(w), A_-(w)$. After running a parameter sweep over all these values, we identified the range of values for which our simulation of the experiment bore resemblance to the experimental STDP curve [Figure 8].

Panel **a** of figure 8 shows our simulation of the Haas, Nowotny, and Abarbanel 2006 experiment using the differential equations in 9 and 10. After simulating the entire network where all the IE synapses are show iSTDP, we saw that it took a lot of time to see a discernible difference in the weights of the network. It would would take of the order of hundred minutes (in *insilico* simulation time) to see a difference large enough to show a functional difference in the behavior of the network. This would translate to the order of tens of days in real simulation time. To speed things up with our simulation, we tweaked the STDP curve by changing the value of $\tau_x = \tau_y = 74.0 \text{ msec}^{-1}$, and slightly increasing the peak value of potentiation at 10 msec (because all synapses in the network simulation were potentiating)[Panel **b**, figure 8]. Making these changes to the STDP curve allowed even larger values of $t_{post} - t_{pre}$ to show an increase in weights. Given that most of the time differences in our network simulation ($t_{post} - t_{pre}$) are greater than 10 msec , using the STDP curve shown in panel **b** of figure 8 saved us more than 90 percent of the total simulation time. All the results discussed in the remainder of this thesis were carried out with the parameter values that were used to plot the STDP curve in panel **b** of figure 8.

3.2 Inhibitory STDP gives rise to an asymmetry in network weights

After fixing different parameter values for our STDP function, we applied this learning rule to all the IE synapses in our network and looked at the changes brought about to network structure and function. According to the Haas, Nowotny, and Abarbanel 2006 experiment, apart from being an asymmetric function in time, the STDP function also differs in the extent of potentiation vs. depression. The magnitude of the potentiation peak is greater than the magnitude of the depression peak, both of which are located at around 10 msec from the center.

Because of this inherent asymmetry in potentiation vs. depression, one would expect a greater fraction of IE synapses to undergo potentiation as opposed to depression. As expected, because of the domineering effect of potentiation over depression, we see that all the synapses in the network potentiate. However, the extent of potentiation was different for different synapses.

For this simulation, all the neurons in the network were kept in a hyperpolarized state

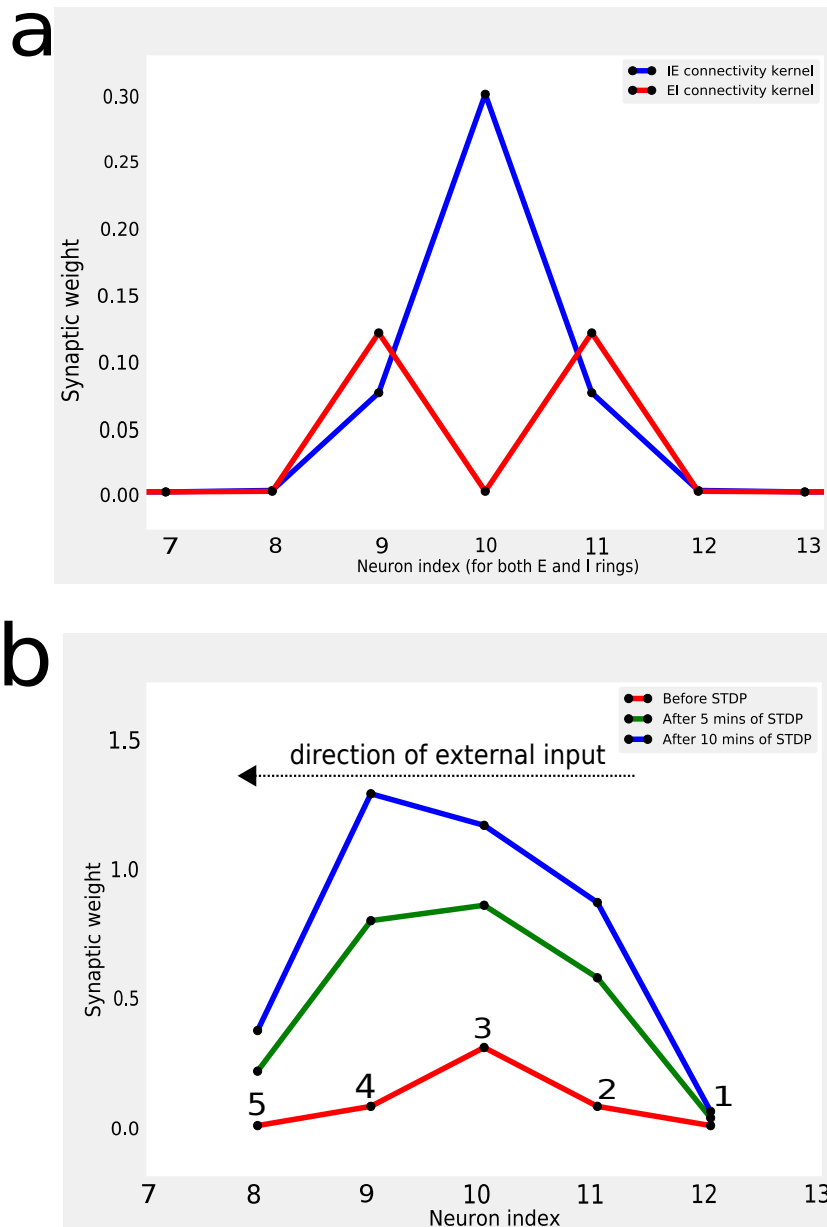


Figure 9. Connectivity kernels - before and after STDP. **a.** IE and EI connectivity kernels for neuron index = 10 (on both E and I rings) before STDP i.e. for a symmetric network. **b.** Changes in the IE connectivity kernel at different stages of STDP (measured in mins). The external input moves from the right to the left. The numbers above the red kernel (before STDP) indicate the different labels assigned to positions on the outgoing connectivity of an I neuron. These positions will be used in figure 10.

by injecting a negative DC current. This was done to ensure that all inhibitory neurons fire only in the presence of an external current greater than a certain value, and all Stellate cells fired only after the rebound after inhibition from the interneurons. This behavior of the Stellate cells in our network agrees with previous research that Stellate cell networks can generate grid fields through the rebound after inhibition paradigm

(Hasselmo and Shay 2014). Additionally, we imposed a time-varying external input of 8 Hz (discussed in 2.3) on the inhibitory interneurons of the network. The external input frequency (εHz) was kept the same as the theta drive frequency (θHz) so as to allow the peak of every theta cycle to coincide with the external input current. The concomitance of the peak of the theta rhythm and the DC external drive was a result of their similar frequencies.

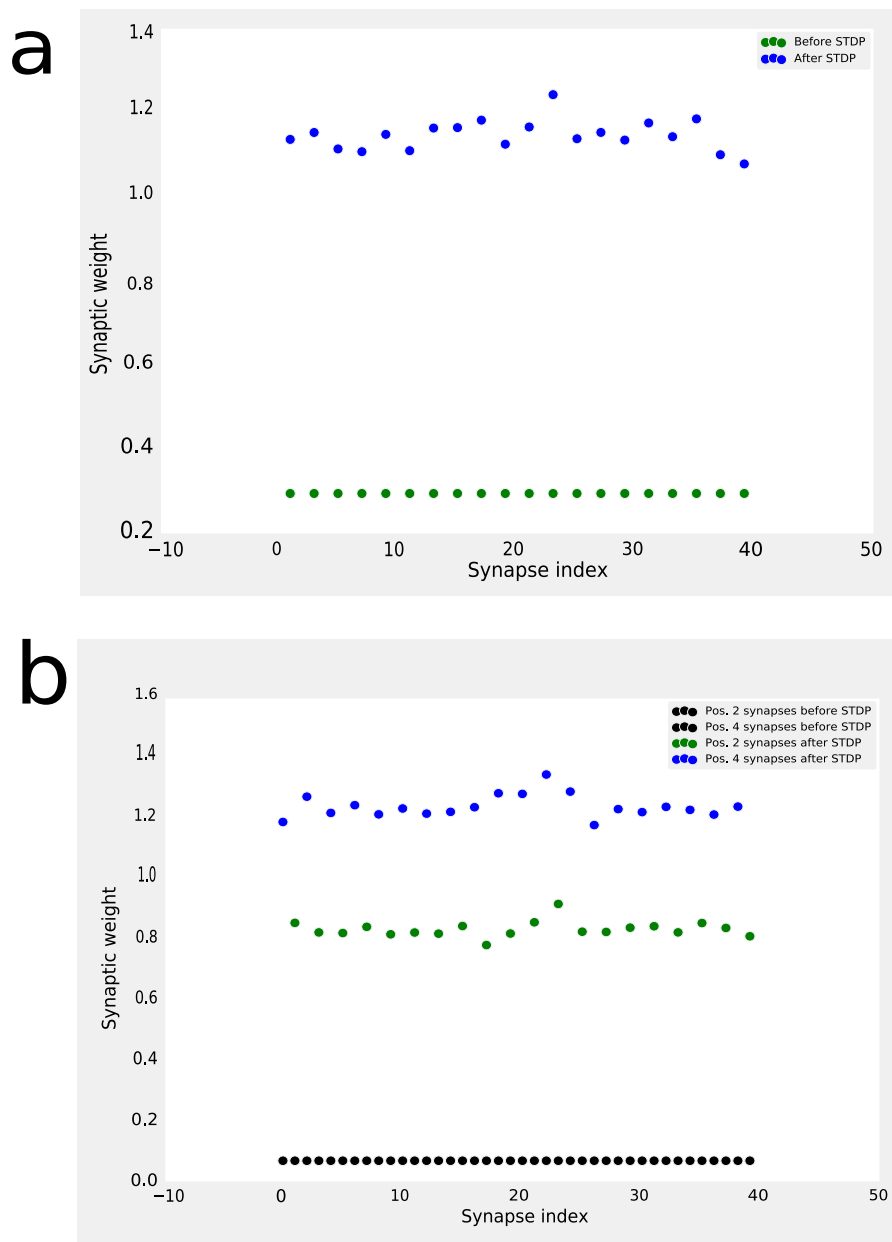


Figure 10. Changes brought about by STDP in the network. **a.** The change in peak value of the *IE* connectivity kernel (position 3) for all the inhibitory neurons in the network after 10 mins of STDP. **b.** The change in weight of all the synapses present in position 2 and position 4 of the *IE* kernel for the entire network.

The need for an external drive arose because we initially started off with a completely symmetric network. Thus, without an external drive, activity wouldn't propagate along a particular direction. Rather, one would observe a random firing order of neurons. One can think of this external drive to neurons as a signal received from other regions of the brain. This could be a signal such as the velocity at which the animal runs, position or tactile cues. Indeed, such signals to stellate cells in the medial entorhinal cortex have been identified and documented in spatial navigation literature. The Haas, Nowotny, and Abarbanel 2006 protocol lasted for a duration of 3-5 *mins*, in realistic biological networks one can expect to see changes brought about by STDP at timescales of tens - hundreds of minutes. Thus, we ran our simulation, with *IE* synapses obeying an inhibitory STDP rule for a duration of 10 *mins*.

After 10 *mins*, we noticed the following changes. First and foremost, our dual ring architecture allowed all the *IE* synapses to potentiate. However, this might simply be an artefact of the inherent asymmetry between potentiation and depression in the STDP curve. More importantly, there was a difference in the extents to which the synapses potentiated. After careful observation, we were able to see that the synapses in the direction of the external input potentiated more when compared to synapses that were oriented in a direction opposite to the external input [Figure 9 and 10]. This induced a very well-defined asymmetry in the system caused by the direction of activity propagation. One could say that as the animal repeatedly moves in one direction, the synapses that correspond to movement in that direction potentiate more than other synapses.

3.3 Learning causes a shift of the robust regime in frequency space

Networks with asymmetry induced by iSTDP had two salient features, **a.** these asymmetric networks appeared to be a lot less robust compared to symmetric networks that were driven by an external input, and **b.** as the extent of asymmetry in the network increased, the speed with which the activity wave spread across the network increased [Figure 15].

A possible reason for the low robustness, mentioned in **a** could be that because asymmetry increases the speed of activity propagation across the ring, this change in speed doesn't match with the onset of the external input to the neuron. In other words, the external input frequency doesn't synchronize with the natural frequency of activity shift that is defined by the weights of the network, this loss of synchronization leads to the activation of different neurons at the same instant of time, and ultimately a de-

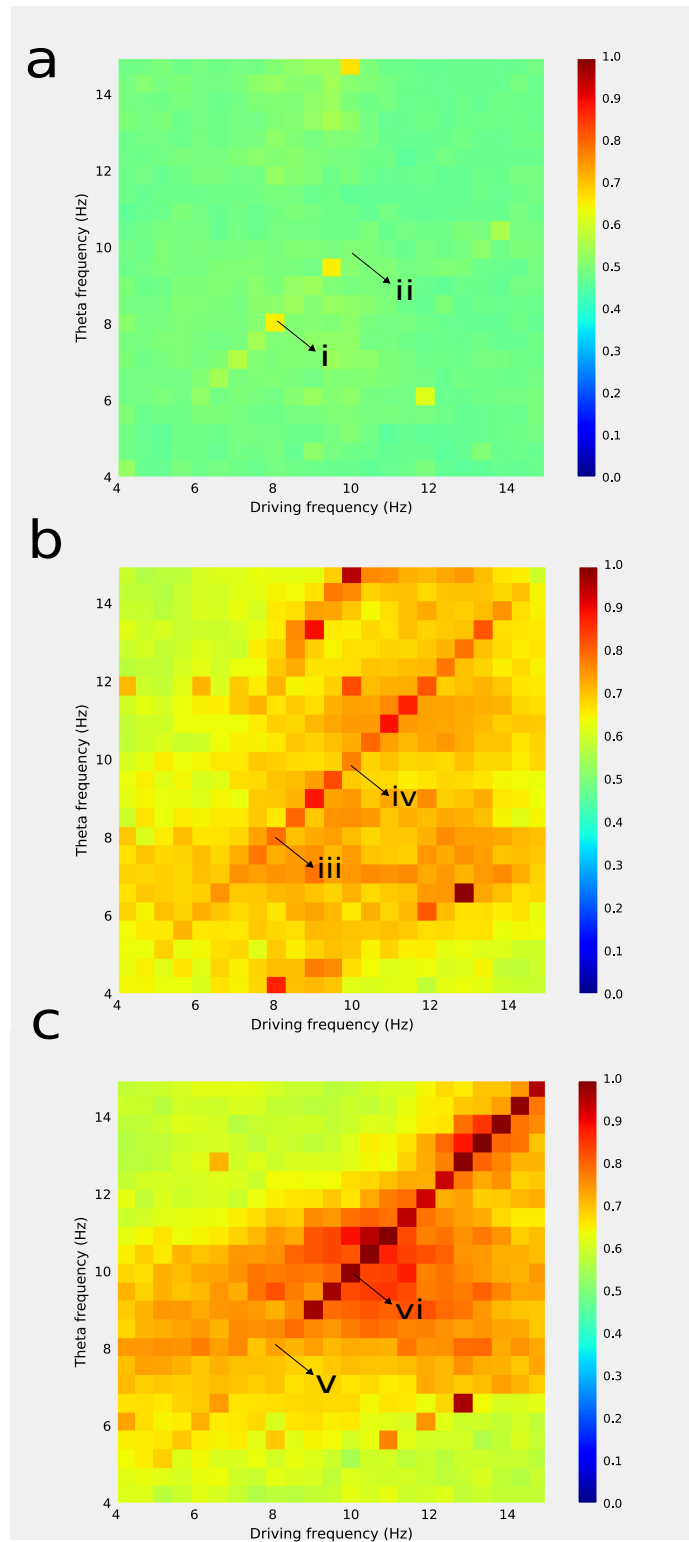


Figure 11. STDP shifts the robust regime to higher values in frequency space. **a**, **b** and **c** are robustness matrices for 0 sec, 30 sec and 180 sec of STDP respectively. The x-axis and y-axis in each of these cases are the frequency of external input (ϵ), and frequency of theta drive (θ), respectively. Each square of the matrix is a value of robustness measured over 10 different trials of the network (refer to 3.3 for details).

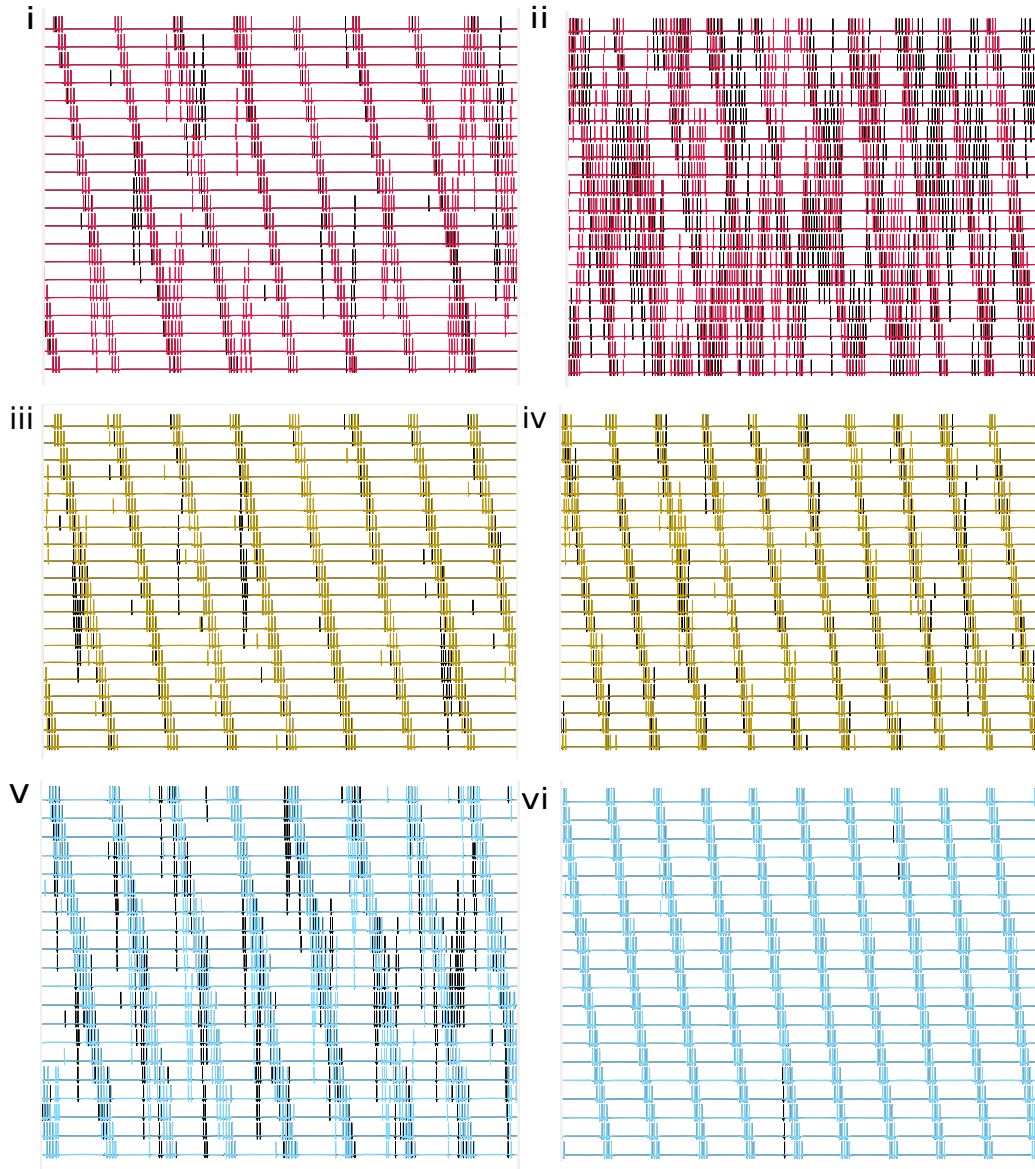


Figure 12. Panels *i*, *ii*, *iii*, *iv*, *v* and *vi* show the behavior of the entire network for the designated squares labelled in figure 11. Panels *i*, *iii* and *v* are neuronal traces for $\theta = \varepsilon = 8Hz$ for matrices **a**, **b** and **c** respectively in figure 11. Panels *ii*, *iv* and *vi* are neuronal traces for $\theta = \varepsilon = 10Hz$ for matrices **a**, **b** and **c** respectively in figure 11. It is evident that $\theta = \varepsilon = 10Hz$ is more robust for asymmetric networks and $\theta = \varepsilon = 8Hz$ is more robust for symmetric networks, the implications of this observation will be discussed in section 3.4.

crease in the robustness of the wave of activity.

To test this hypothesis, we simulated 10 trials for 529 different combinations of theta drive frequency (θHz) and external input frequency (εHz). We compared these simulations for both symmetric and different asymmetric network topologies at 30 *secs* and 180 *secs* of STDP. The data was represented in the form of a matrix of 529 squares (23×23), with each square representing a different value of θ and εHz . For each par-

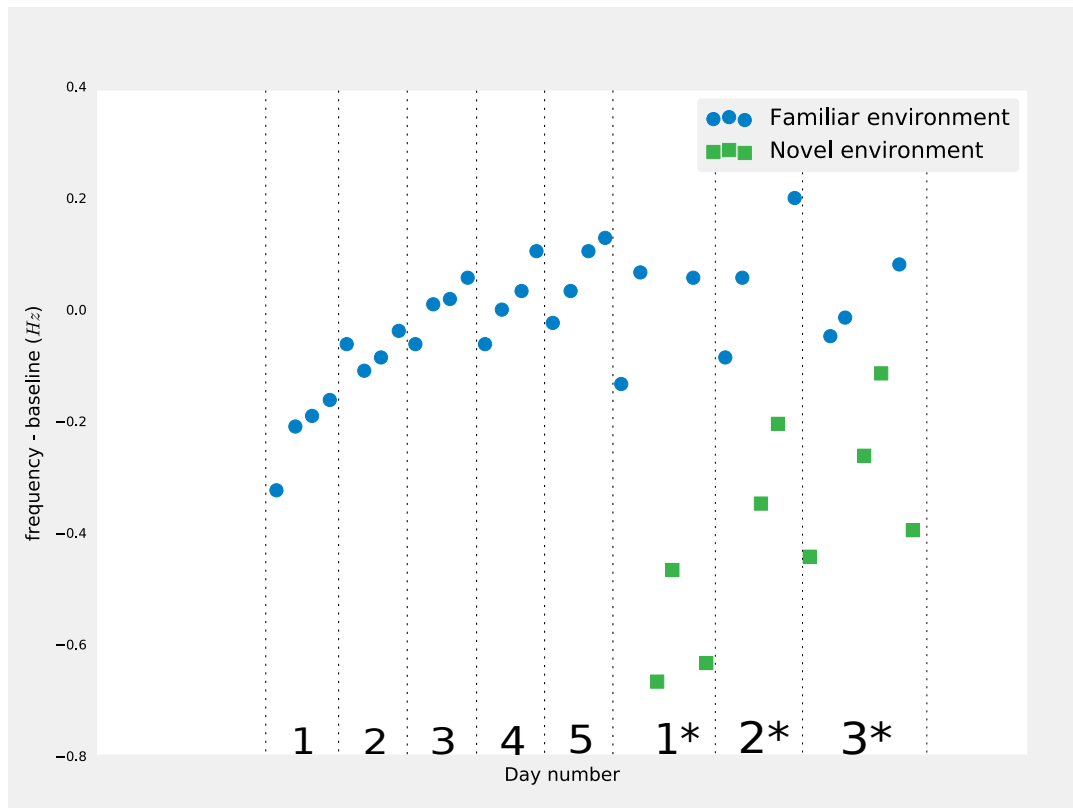


Figure 13. A figure panel adapted from Jeewajee et al. 2008 that shows the decrease in frequency of theta rhythm (θ Hz) as the animal is shifted to a novel environment. The x-axis shows the number of days the animal is kept in an environment. All days with an asterisk (1*, 2* and 3*) indicate days that correspond to the transfer of the animal to a novel environment. The y-axis is a measure of the change in θ in comparison to the baseline value of θ when the animal is familiarised with its environment. For the variance in data point values and the exact conditions in which the experiment was performed, the reader can consult Jeewajee et al. 2008.

ticular case, i.e. a given value of (θ, ε) , we measured the robustness of the network by using the synchronization measure described in section 2.5.

After calculating the synchronization measure over 10 trials for 529 different cases, and representing these values in the form of a square matrix, it was clearly visible that the stable region among the 529 different squares had shifted to higher frequency values, i.e. the robust regime in frequency space had moved further to the upper right corner in the frequency matrix. These observations agree with previous experiments that observed that the frequency of theta oscillations drops to lower values when the animal is introduced to a novel environment and gradually increases as the animal gets familiarised with its environment (Jeewajee et al. 2008)[Figure 13]. A very recent paper which studied brain rhythms in freely-moving humans makes the case for higher frequency theta rhythms during movement or active exploration (Yassa 2018). Our theory predicts that the possible reason for this increase in theta drive frequency with

increasing familiarity could be the need to produce robust grid cell sequences. We propose that the changing network topology as the animal explores its environment, is the driving force behind this shift in theta frequency values.

3.4 Asymmetry in the network connectivity reduces the width of neuronal bursts and defines a direction of propagation

Given that inhibitory STDP introduces an asymmetry - hence favoring one direction of propagation over the other, one immediately expects to see changes in network activity that are a result of this newly generated asymmetry. In section 3.3 we showed that asymmetry effected through STDP can change the range of theta frequencies for which the network is stable - a very important functional change. As STDP acts on the synapses in the network, the amount of asymmetry gradually changes as a function of time. We took snapshots (observed synaptic weights) of all the synapses at different timepoints of the simulation, at intervals of 10 *sec*, and used these values of synaptic weights to set up different simulations. All the snapshots of the network were within the first 200 *secs* of the STDP simulation. We did this because after the first 200 *secs* of the simulation, there was a significant shift in the robust regime, as discussed in section 3.3. We found that after the first 200 *secs* of the simulation, one had to increase the value of theta frequency to ensure stable firing of the network.

The simulations discussed in sections 3.2 and 3.3 were carried out in the presence of an external input. In order to test the effects of asymmetry in the absence of an external input, we changed the value of the DC current injected to Inhibitory neurons to a positive value. This enabled inhibitory interneurons to fire of their own accord, and Stellate cell firing to be guided by rebound after inhibition from neighboring interneurons, as explained in section 2.3. Removing the external input to individual neurons allowed us the study the sole effects of asymmetry on network behavior.

We observed that with increasing levels of asymmetry the average width of neuronal bursts and the value of inter-burst interval (IBI) decreased [Figure 14]. Naturally, this also allowed for activity to spread faster across the ring. These plots show that asymmetry alone can bring about a 36 percent decrease in IBI. However, the absence of an external input to the inhibitory neurons is analogous to the condition where the animal is stationary (no velocity input to the mEC). To mimic the conditions experienced by an navigating animal in reality, we must account for **a.** an external signal which plays the role of inputs from other brain regions to the mEC and **b.** The increase in frequency of theta input to the mEC, which has been found in experiments (Jeewajee et al. 2008,

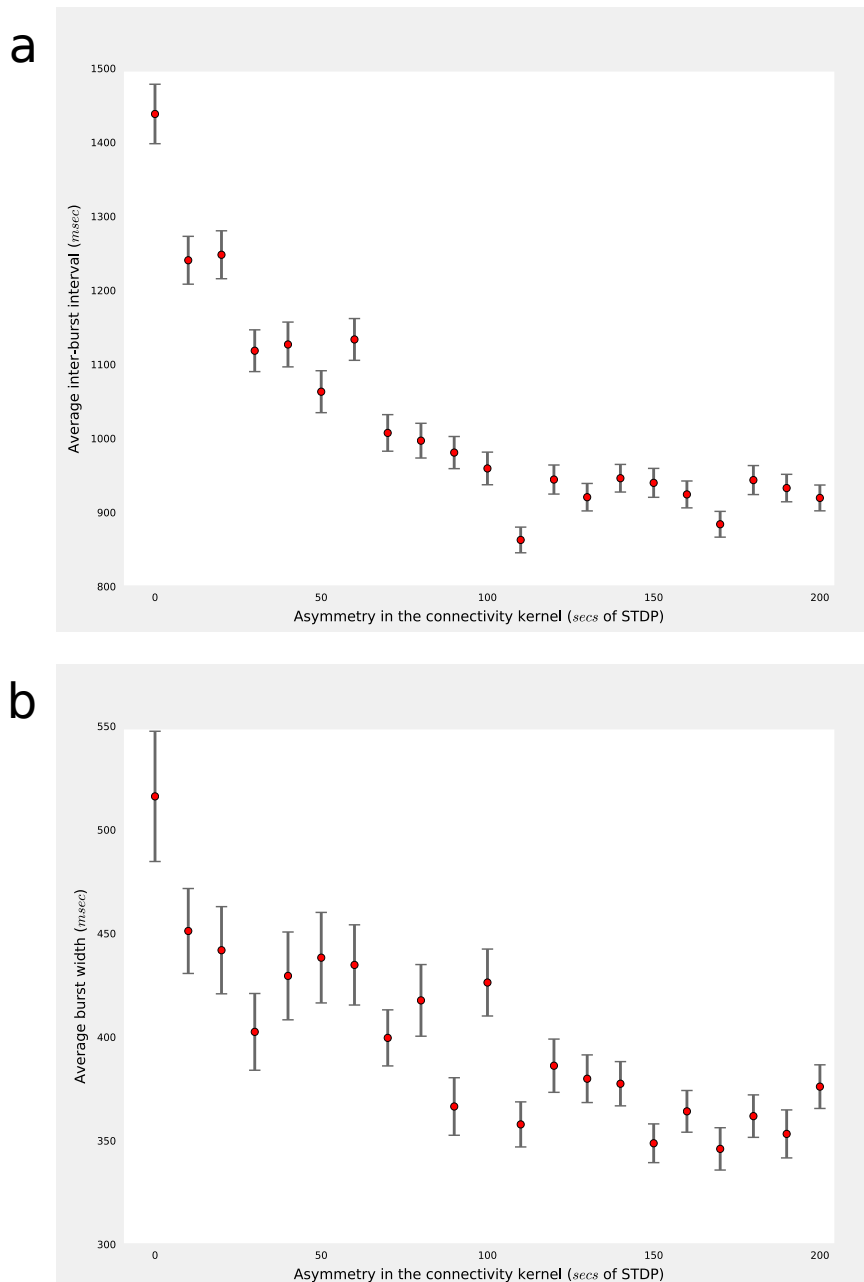


Figure 14. *Asymmetry increases the speed of activity propagation across the ring. a. A plot of the average inter-burst interval of all the neurons in the network vs. the amount of asymmetry in the ring (measured as secs of STDP acted. b. A plot of the average burst width of all the neurons in the network vs. the amount of asymmetry in the ring (measured as secs of STDP acted.)*

Yassa 2018) and in our simulations.

The inclusion of an external input to the system introduces order in the pattern of firing. Propagation of sequences in one direction ensures that we are studying the motion of an animal traveling along a linear track in one direction. With a concomitant increase in

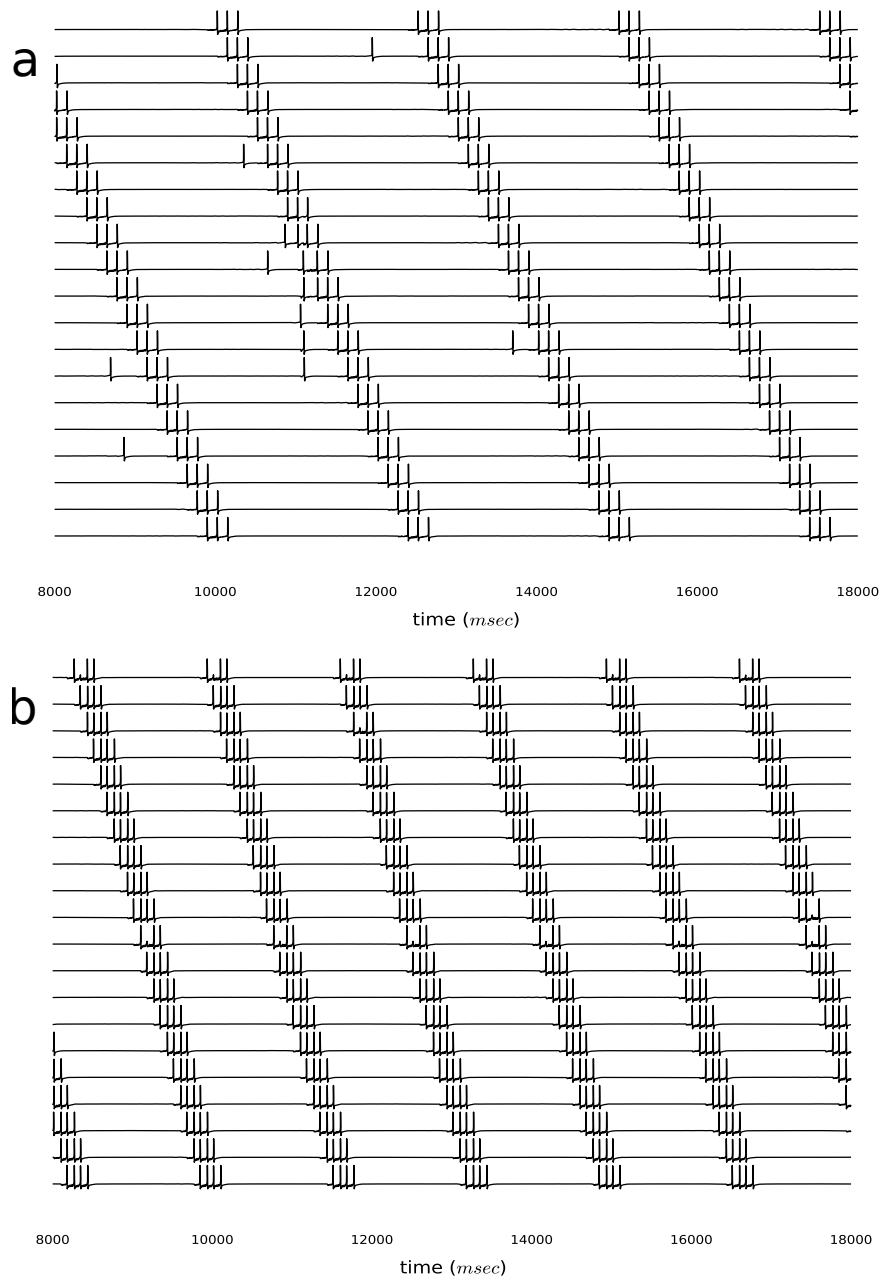


Figure 15. *Propagation of sequences in the presence of an external input. a. A snapshot of network activity for a completely symmetric network (0 secs of STDP), for this simulation $\theta = \varepsilon = 8\text{Hz}$. b. A snapshot of network activity for an asymmetric network (180 secs of STDP), for this simulation $\theta = \varepsilon = 12\text{Hz}$*

the frequency of theta oscillations, we see a very clear decrease in the burst width and IBI. This reduction in the value of burst width and IBI increased the speed of activity propagation across the network. Since the animal moves in a straight line, each IBI corresponds to the distance between the start of one receptive field to the start of the next. Thus, the shrinking of IBIs can be thought of as direct evidence that the spatial scale of the grid pattern decreases as the animal spends more time in its environment

- allowing STDP to act. This is the most important claim of my thesis and sums up our explanation of the phenomenon of grid field maturation. We put forth the following ideas: **a.** The animal "learning" the environment is represented as structural changes in the network connectivity brought about by iSTDP **b.** The structural changes cause an asymmetry in the synaptic connections, as the animal favors one direction of travel over the other **c.** The induced asymmetry in the network connectivity changes the functional behavior of the system, in that, higher frequency values of external inputs are preferred **d.** Higher frequency inputs in conjunction with the asymmetry induced by STDP are responsible for the changes in properties of grid cell firing as the animal becomes familiar with its environment, i.e. the decrease in spatial scale of the grid pattern.

4 Discussions

4.1 Network connectivity - Experiments, Results and Inferences

In this study, we have shown that a network with a dual-ring architecture, with a certain network topology and external inputs can mimic the changes shown by grid cell networks. In the following section, we will briefly talk about the experiments that have led us to construct the network in the following manner.

Earlier studies have found that Stellate cells in the mEC do not receive excitatory input, and connect to each other via inhibitory intermediaries, forming a recurring inhibitory network (Couey et al. 2013). Couey et al. 2013 demonstrated that a model employing this connectivity framework could produce hexagonal grids. A recent study used three-dimensional electron microscopy to create dense reconstructions of local presynaptic axons in layer II of the mEC found the existence of cellular feedforward inhibitory networks (Schmidt et al. 2017). Schmidt et al. 2017 found that Stellate cells selectively synapse onto inhibitory interneurons which inhibit other excitatory neurons in the mEC, primarily pyramidal neurons. Simulations performed using this type of network connectivity have shown that these neuronal networks can produce precisely regulated firing patterns. These experiments allow us to draw two important inferences about the connectivity of the mEC: **a.** There are almost none/very few excitatory-excitatory connections (EE synapses) in the mEC (Couey et al. 2013), **b.** Since very few/almost no feedback connections exist in the mEC, there will be minimal overlap in the connectivity kernels of excitatory and inhibitory neurons that are directly connected (E neurons and I neurons positioned next to each other in figure 5).

In keeping with these experimental findings, one can design the network connections in one of the two ways shown in figure 16. The two connectivity profiles shown in figure 16 are the only two possible ways of connecting the network assuming that the outgoing connectivity of a neuron (E/I) is either nearest-neighbour connected or a slight offset from nearest neighbour connectivity. The reason we picked a bimodal kernel (peaks around the central peak), as opposed to an unimodal kernel is because we didn't want to inherently bias the propagation of neuronal activity in one direction of the ring over the other. Consider case **b.** of figure 16, in such a connectivity paradigm each Stellate cell makes a single interneuron fire (neuron at the peak of the EI kernel). Now, upon firing, this interneuron will proceed to activate two Stellate cells, as dictated by the IE kernels that branch off into two opposite directions of the ring. So, in case **b.** of figure 16 it would not be possible to ensure that the activity is propagated solely in one direction. Thus, this type of connectivity would not be a good way to study the

motion of an animal that moves in a single direction along a straight line. Considering this fact, we chose to model the synaptic connections in our network according to the connectivity scheme of case **a.**, figure 16. The exact kernel with the values of synaptic weights used (before STDP acts on the network) has been shown in panel **a** of figure 8. The peak weights and the width of the Gaussian functions (for connectivity kernels) were picked after doing a parameter sweep for peak heights and widths; we selected the connectivity kernel that gave us a robust propagation of network activity only in the presence of an external theta drive to the network.

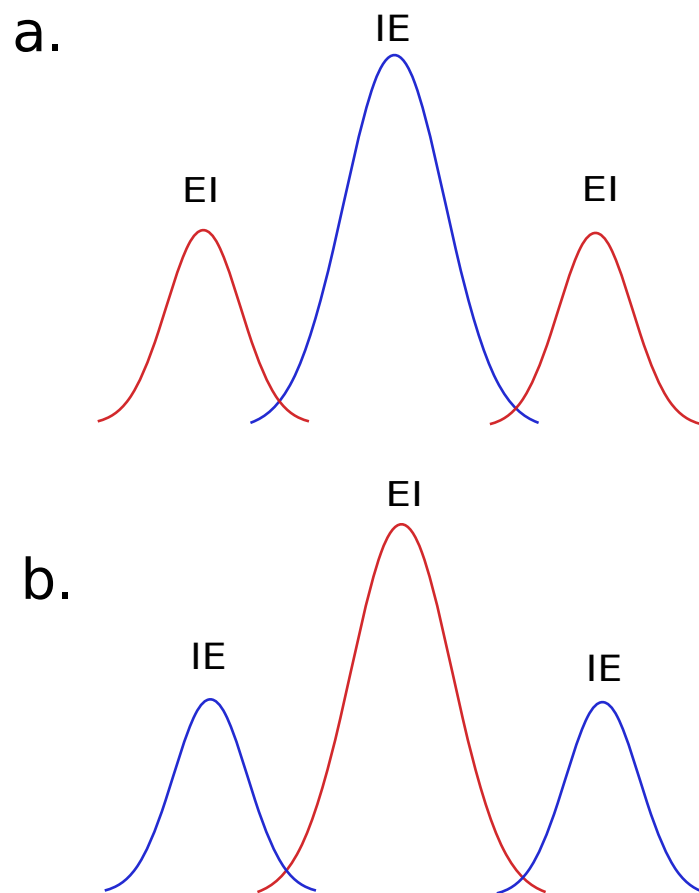


Figure 16. A schematic illustrating the two possible types (**a** and **b**) of connectivity kernels we could have used in our network. Both *IE* and *EI* connectivity kernels have been modelled as Gaussian functions. Blue - *IE* connectivity kernel, Red - *EI* connectivity kernel.

Many other experiments looked at inputs to the Entorhinal Cortex from the medial septum. Studies have found that theta oscillatory inputs ($4\text{ Hz} - 12\text{ Hz}$) from the medial septum (MS) are important for maintaining the robustness of the grid pattern formed by neurons of the mEC (Koenig 2011). These studies led to the belief that theta input from the MS plays a very important role in spatial navigation. Bats are the only known exception to this; bats show robust grid field formation even in the absence of

continuous theta-band oscillations (Yartsev, Witter, and Ulanovsky 2011). It has been found that inputs from the medial septum selectively inhibit Inhibitory interneurons in the mEC, through GABAergic synapses (Gonzalez-Sulser et al. 2014). In accordance with these experiments, we provide theta rhythmic input to all the inhibitory neurons in our network.

In our work, we suggest a possible mechanism to explain the functional changes that learning brings about in a network. We put forth the idea that Inhibitory Spike-timing dependent plasticity, a phenomenon shown to exist in the IE synapses of the mEC, could induce long lasting changes in grid cell circuits that change the firing properties of the circuit, and thus, each individual grid cell. Our simulations show that iSTDP alters the weights of the network in such a way that it makes them more asymmetric with time. We show that this induced asymmetry can explain many experimentally observed behaviors of grid cell networks.

We understand that there might be other mechanisms that could be responsible for the functional changes observed in grid cell firing properties as the animal learns its environment. One possible alternative could be that learning brings about changes in the networks present in areas closely associated to the mEC, and the input of these areas to the mEC is changed, which causes the changes in the firing patterns of grid cells. Another possibility is that the sharper fields, and reduced inter-grid distance could be an effect of reducing the variability in the inputs that feed into the mEC from areas like the medial septum (theta rhythm), hippocampus etc.

4.2 Extending our study to 2D trajectories

We understand that restricting ourselves to the study of linear trajectories does not do justice to the problem at hand. In reality, unless the animal is forced by a task/physical boundaries, it is very unlikely that the animal will restrain itself to moving along a straight line in only one direction. So, how do we solve the problem of motion in more than one direction? To account for this, we propose the following: keep a different subset of neurons that code for each direction. Figure 17 shows how it is possible to code for movement in two directions by keeping two subsets of neurons - east-going and west-going neurons. The existence of two different rings of Stellate cells that code for both directions ensures that each direction gets an independent representation in the neuronal network. So, if the animal runs east more times than the animal runs west, then the east-going ring of neurons will have a greater level of asymmetry compared to the west-going ring of neurons.

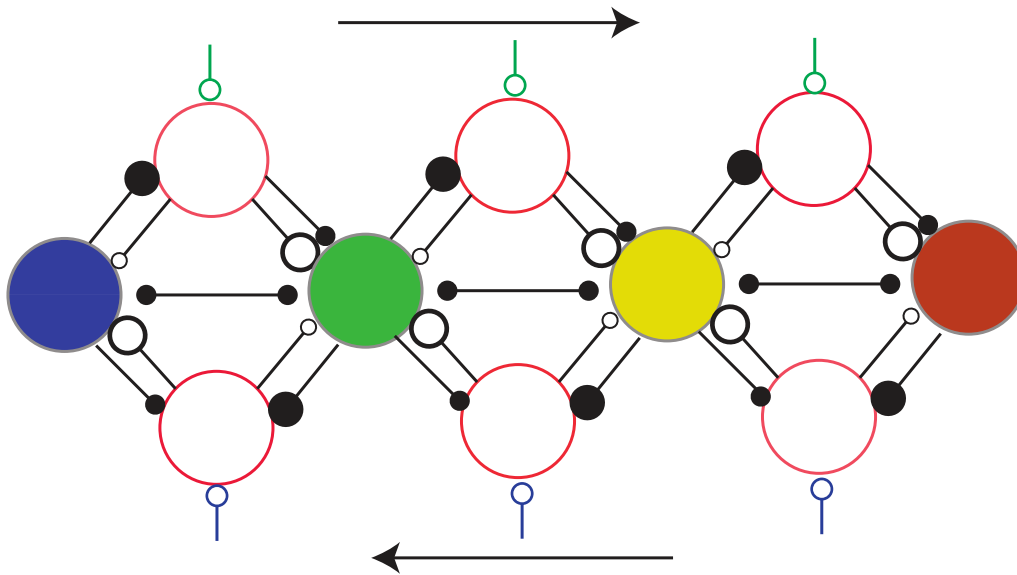


Figure 17. The circles with solid colors (blue, green, yellow and red) represent Inhibitory Interneurons that have an all-all connectivity (all the II connections haven't been shown here.) The hollow circles with a red outline represent Stellate cells. There are two different groups of Stellate cells, one group that receives input when the animal travels eastwards (receive green input) and the other group that receives input when the animal travels westwards (receive blue input). The arrows on the top and bottom represent the direction in which the animal is moving, i.e. the upper row of Stellate cells are active when the animal is travelling rightward, and the bottom row of Stellate cells will be active when the animal is traveling leftward.

One can similarly account for all four cardinal directions by dedicating a separate ring of neurons for each of the directions. The line of thinking, however, can only extend to a finite number of directions. Using such a scheme, it would become difficult to code for motion when the animal doesn't restrict itself to straight-line paths. If the animal travels along a curve, then one possible way to code for such movement would be to decompose the curve into straight paths by replacing every point on the curve with a tangent to that point. While such a recipe does seem to offer a solution to the problem, it would involve the constant switching of activity between neurons on different rings via an external current source. Also, there is no guarantee that such a network would generate grid fields and show the maturation of these grid fields with environmental familiarity.

The field of Spatial navigation doesn't have a satisfactory answer to the riddle of navigation in two dimensions. The two dominant classes of models - Continuous attractor networks (CANs) and Oscillatory Interference networks (OINs) have their own shortcomings. CANs make use of network topologies that are yet to be verified, and existing models of CANs use overly-simplified neuron models that ignore the internal dynamics

and rich variation in spiking behavior across different neurons types (Burak and Fiete 2009, Giocomo, M.B. Moser, and E.I. Moser 2011). OINs make unrealistic assumptions about the phase of incoming oscillatory input to the cells (Hasselmo and Shay 2014, Blair, Gupta, and Zhang 2008). The existence of grid fields in the absence of a continuous theta oscillation (Yartsev, Witter, and Ulanovsky 2011), weakens the case for OINs as the mechanism behind grid field generation. In summary, each class of models has its own drawbacks. The topic of grid field formation is one of great interest and is heavily disputed, unless there is more substantiating experimental evidence, it isn't possible to ascertain the exact mechanism used by cells to represent space.

4.3 Similarities with hippocampal sequences and memory consolidation

In section 3.4 we showed that as the network becomes more asymmetric, the width of neuronal bursts and the inter-burst interval decreases. Apart from causing functional changes in the behavior of the network, we wanted to see whether asymmetric networks could maintain the propagation of activity (along a direction of the ring) in the absence of an external input. To do this we simulated networks at different stages of STDP (seconds for which STDP was active). After about 10 *mins* of STDP, we observed that even in the absence of an external input, the direction of activity propagation remained the same. In other words, the asymmetry caused by STDP left a long-lasting change on the behavior of the network, in that it favored one direction over the other [Figure 18].

Previous studies wherein the subject is asked to mentally navigate across a virtual landscape have shown us that that subjects are able to form cognitive maps, and successfully navigate using these maps in the absence of tactile and motion cues (Doeller, Barry, and Burgess 2010, Deuker et al. 2016). These studies tell us that position and velocity information might not be necessary to successfully navigate about a landscape once the subject has gained reasonable familiarity with its environs. The results of our simulations provide a plausible explanation for this experimental observation. The animal's 'familiarity' with its environment is a measure of change brought about in neuronal networks in the hippocampal formation through learning. We put forth the idea that Inhibitory STDP present in the *IE* synapses gives rise to asymmetries in network connectivity that could explain the ability of animals to successfully navigate in the absence of additional cues.

However, I believe that one must look at this result with some skepticism. Although

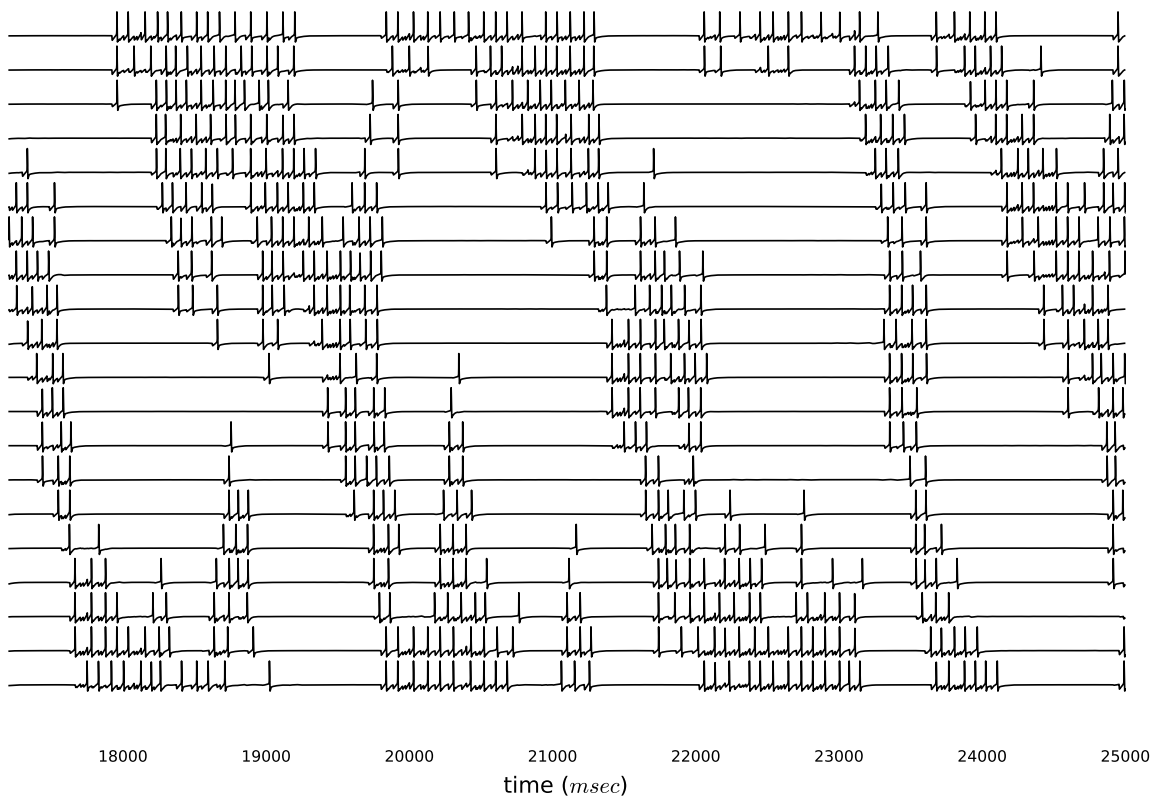


Figure 18. *Propagation of sequences in an asymmetric network (10 mins of STDP) in the absence of an external input.*

sequences that propagate along the same direction of the external input can be found in figure 18, these sequences are not the same as the sequences obtained in the presence of an external input [Figure 15]. The primary distinction between the two sequences is the fact that the sequences obtained in the absence of an external input are much less robust, i.e. the number of spikes per burst, the onset of a burst and the overlap between the bursting phases of neighbouring neurons are highly variable, and appear to be governed by extraneous stochastic forces. Thus, one must be careful before making the claim that these firing patterns of Stellate cells could represent the motion of an animal through space.

Having said that, one can draw some very interesting parallels between the sequences found in figure 18 and the sequences observed in hippocampal place cells. The sequences obtained in the absence of an external input represent the behavior of Stellate cells when the animal is either sleeping or in an awake resting state. In states of sleep/awake resting, the behavior of place cells is very interesting: place cells activity during sleep mimics the place cell activity during motion. In other words, the ensemble of place cells that was active during active exploration is also active during states of awake resting and sleep (Pavlides and Winson 1989, Skaggs and McNaughton 1996,

Louie and Wilson 2001). However, there are two important distinctions between the sequences during active exploration and sequences during sleep/awake resting, **i.** The sequences during sleep and awake resting can be either in the original direction of propagation (forward replay) or in the opposite direction (reverse replay) (Diba and Buzsáki 2007, Buzsáki 2015) and **ii.** These sequences appear to be temporally compressed, the entire place cell ensemble firing in about 40 *msec* - 100 *msec*.

Most replay events co-occur with a high frequency (100-250 *Hz*) burst that manifests itself in the local field potential (LFP) of the hippocampus (Buhry, Azizi, and Cheng 2011). These bursts were termed as Sharp-wave ripple sequences (SWRs), a detailed review of almost every aspect of SWRs can be found in Buzsáki 2015. Initially, studies found a strong correlation between the occurrence of SWRs and memory consolidation, the storage of memories of real-life events (Axmacher, Elger, and Fell 2008, Dupret et al. 2010). It was subsequently verified that SWRs are required for the consolidation of episodic memories, this was done in a number of very elegant experiments where the authors disrupted the formation of SWRs through external means (Girardeau et al. 2009, Ego-Stengel and Wilson 2010, Jadhav et al. 2012). This is where the field of SWRs currently stands, a causal link between SWRs and memory consolidation is almost irrefutable. However, the exact mechanism by which SWRs lead to the consolidation of memories still remain unknown. The most popular hypothesis that dominates the field currently is that replay events (co-occurring with SWRs) happen in timescales that have previously been shown to induce LTP (T.V.P. Bliss and Lømo 1973, T.V. Bliss and Collingridge 1993). However, this hypothesis needs verification.

Sequences in our network in the absence of an external drive resembles place cell replay events in sleep and awake resting states of the animal. Consider the relatively fast burst of neurons that occurs at around 24,000 *msec* in figure 18, the total duration of this burst (across the entire ensemble of Stellate cells) is of the order of 100-200 *msec*. This timescale of activity discharge for an ensemble is comparable to that observed during SWRs in the hippocampus. We see a lot more of such fast discharges in networks with asymmetries. However, due to various constraints, we have not been able to quantitatively study the properties of these fast-sequences and explore this area of the project. The existence of such fast bursts in our asymmetric networks, and the noticeable direction of activity propagation, is very encouraging - tempting us to draw comparisons between our model and Hippocampal place cell sequences. It is quite possible that network topology is the reason for behind the formation of SWRs in the Hippocampus. However, without more substantiating evidence, one can only speculate.

5 Appendices

5.1 Neuronal parameters

Stellate cells

- **Resting potential of the neuron (at the start of the simulation):** Values for a single neuron are drawn from a Normal distribution where $\mu = -61.2$, $\sigma = 12.5$. The value of μ, σ of resting potentials of the entire Stellate cell population was taken from the data provided in Haas, Nowotny, and Abarbanel 2006.

- **Values of gating variables at the start of the simulation:** $m = 0.0224224$, $n = 0.1.3519$, $h = 0.954963$, $p = 0.0678057$, $r_s = 0.118111$, $r_f = 0.0779264$

- **Parameters used in equations 3 and 4:**

$$\alpha_m(V) = -0.1(V + 23)/e^{-0.1(V+23)-1}$$

$$\beta_m(V) = 4e^{-(V+48)/18}$$

$$\alpha_h(V) = 0.07e^{-(V+37)/20}$$

$$\beta_h(V) = 1/(e^{-0.1(V+7)} + 1)$$

$$\alpha_n(V) = -0.01(V + 27)/(e^{-0.1(V+27)} - 1)$$

$$\beta_n(V) = 0.125e^{-(V+37)/80}$$

$$\alpha_p(V) = 1/(0.15(1 + e^{-(V+38)/6.5}))$$

$$\beta_p(V) = e^{-(V+38)/6.5}/(0.15(1 + e^{-(V+38)/6.5}))$$

$$r_{f,\infty}(V) = 1/(1 + e^{(V+79.2)/9.78})$$

$$\tau_{r_f}(V) = 0.51/(e^{(V-1.7)/10} + e^{-(V+340)/52}) + 1$$

$$r_{s,\infty}(V) = 1/(1 + e^{(V+2.83)/15.9})^{58}$$

$$\tau_{r_s}(V) = 5.6/(e^{(V-1.7)/14} + e^{-(V+260)/43}) + 1$$

- The initial values of all the currents, namely I_{Na} , I_k , I_L , I_{NaP} , I_h , I_{DC} , I_{ext} are all set to 0. The value of current to the cell through an ion channel evolves according to the equations specified in equation 2.

- **Values of maximum conductance and reversal potentials for ion channels**

All maximal conductances are in mS/cm^2 and all reversal potentials are in mV .

$$G_{Na} = 52, E_{Na} = 55$$

$$G_K = 11, E_K = -90$$

$$G_L = 0.5, E_L = -65$$

$$G_h = 1.5, E_h = -20$$

$$G_p = 0.5$$

- The value of capacitance of the neuron is set to $1 \mu F/cm^2$

- **External DC input given to Stellate cells**

Periodic pulse input - I_{ext}

The periodic pulse input is a current defined to mimic the effects of a constant external DC to all the Stellate cells of the network. The equations describing the periodic pulse input to the neurons are:

$$I_{ext} = \begin{cases} P_{min} & t < t_{start} \\ P_{max} + (P_{min} - P_{max})e^{-(t-t_{start})/\tau_{rise}} & t \in [t_{start}, t_{end}] \\ P_{min} + (P_{max} - P_{min})e^{-(t-t_{end})/\tau_{fall}} & t > t_{end} \end{cases} \quad (16)$$

where,

t = time

t_{start} = temporal onset of current

t_{end} = temporal termination of current

It is important to note that the values of t_{start} and t_{end} are periodic. That is,

$$t_{start} = t_1, t_1 + \Gamma, t_1 + 2\Gamma + \dots$$

$$t_{end} = t_2, t_2 + \Gamma, t_2 + 2\Gamma + \dots$$

where,

t_1 = First onset of periodic pulse, t_2 = First termination of periodic pulse and $t_2 - t_1 = t_{\Delta}$, where t_{Δ} is the duration of the pulse and Γ is the time period of the periodic pulse. The values of the parameters in equation 16 for stellate cells are as follows:

$$\Gamma = 30 \text{ sec}$$

$$t_1 = 1 \text{ sec}$$

$$t_2 = 29 \text{ sec}$$

$$\tau_{rise} = \text{Random number from the uniform distribution } [20.0, 200.0] \text{ msec}^{-1}$$

$$\tau_{fall} = 20.0 \text{ msec}^{-1}$$

In the presence of an external input to the inhibitory interneurons:

$$P_{min} = \text{Random number picked from the uniform distribution } [-4.0, -3.6] \mu A/cm^2$$

$$P_{max} = -2.7 \mu A/cm^2$$

In the absence of an external input to the inhibitory interneurons:

$$P_{min} = \text{Random number picked from the uniform distribution } [-4.0, -3.6] \mu A/cm^2$$

$$P_{max} = 0.2 \mu A/cm^2$$

Inhibitory interneurons

- **Resting potential of the neuron (at the start of the simulation):** Values for a single neuron are drawn from a Normal distribution where $\mu = -61.2$, $\sigma = 12.5$. The value of μ, σ of resting potentials of the entire inhibitory interneuron population was kept the same as the distribution of resting potentials for Stellate cells; this was done for simplicity.
- **Values of gating variables at the start of the simulation:** $m = 0.0224224$, $n = 0.764751$, $h = 0.283859$

- **Parameters used in equations 3 and 4:**

$$\alpha_m(V) = -0.1(V + 35)e^{-0.1(V+28)} - 1$$

$$\beta_m(V) = 4e^{-(V+60)/18}$$

$$\alpha_h(V) = 0.07e^{-(V+58)/20}$$

$$\beta_h(V) = 1/(e^{-0.1(V+28)} + 1)$$

$$\alpha_n(V) = -0.01(V + 34)/(e^{-0.1(V+34)} - 1)$$

$$\beta_n(V) = 0.125e^{-(V+44)/80}$$

- The initial values of all the Currents, namely $I_{Na}, I_k, I_L, I_{DC}, I_{ext}$ are all set to 0. The value of current to the cell through an ion channel evolves according to the equations specified in equation 2.
- **Values of maximum conductance and reversal potentials for ion channels**
All maximal conductances are in mS/cm^2 and all reversal potentials are in mV .
 $G_{Na} = 35, E_{Na} = 55$
 $G_K = 9, E_K = -90$
 $G_L = 0.1, E_L = -65$
- The value of capacitance of the neuron is set to $1 \mu F/cm^2$

- **The behavior of the gating variables**

The excitation variable for the sodium current (m) is assumed to be fast, hence m is substituted by its steady-state values $m_\infty = \alpha_m/(\alpha_m + \beta_m)$.

The behavior of the gating variables h and n obey the following first order differential equations: $dh/dt = \phi(\alpha_h(1 - h) - \beta_h h)$ and $dn/dt = \phi(\alpha_n(1 - n) - \beta_n n)$ where $\phi = 5$.

- **The external current inputs given to the Inhibitory interneurons in the network**

1. *Sinusoidal input - I_{osc}*

The sinusoidal input is given to all the interneurons to mimic the effect of the theta drive from the medial septum to the inhibitory interneurons of the mEC (Koenig 2011, Gonzalez-Sulser et al. 2014). The mathematical form of the sinusoidal input is:

$$\text{Sinusoidal input} = A \sin(2\pi\omega/1000.0 + \Phi)(V - V_{th})$$

where,

$$A = \text{Amplitude of input} = 0.05 \mu A/cm^2$$

ω = Frequency of theta drive = 8 Hz (for all simulations). The frequency of theta drive was varied to obtain figures 11 and 12.

Φ = Phase of incoming input to neuron = 0.0 i.e. all the interneurons receive inputs with the same phase.

V = Membrane potential of the neuron (mV)

V_{th} = Threshold potential of the drive = -80 mV

2. *Periodic pulse input - I_{ext}*

The periodic pulse input (for interneurons) to mimic the effects of both, a constant external DC to all the interneurons of the network, and the shifting external input described in section 3.2. The equations describing the periodic pulse input to the interneurons are the same as those detailed in equation 16.

The values of the parameters used in equation 16 vary depending on whether the periodic pulse current is used as a common DC input or as an external input given to one neuron at a time. The values of the parameters for each of these cases is given below.

- (a) Constant D.C. to all interneurons

$$P_{min} = -3.1 \mu A/cm^2$$

$$P_{max} = -0.05 \mu A/cm^2$$

$$\Gamma = 30 \text{ sec}$$

$$t_1 = 1 \text{ sec}$$

$$t_2 = 29 \text{ sec}$$

$$\tau_{rise} = \text{Random number from the uniform distribution } [20.0, 200.0] \text{ msec}^{-1}$$

$$\tau_{fall} = 20.0 \text{ msec}^{-1}$$

(b) External input given to a single interneuron

$$P_{min} = -0.05 \mu A/cm^2$$

$$P_{max} = 1.0 \mu A/cm^2$$

$$\Gamma = 30 \text{ sec}$$

$t_{\Delta} = 1/\omega \text{ msec}$. For all simulations, except figures 11 and 12, the value of ω was set to 8 Hz, so $t_{\Delta} = 125 \text{ msec}$.

$$\tau_{rise} = 2.0 \text{ msec}^{-1}$$

$$\tau_{fall} = 2.0 \text{ msec}^{-1}$$

5.2 Synaptic parameters

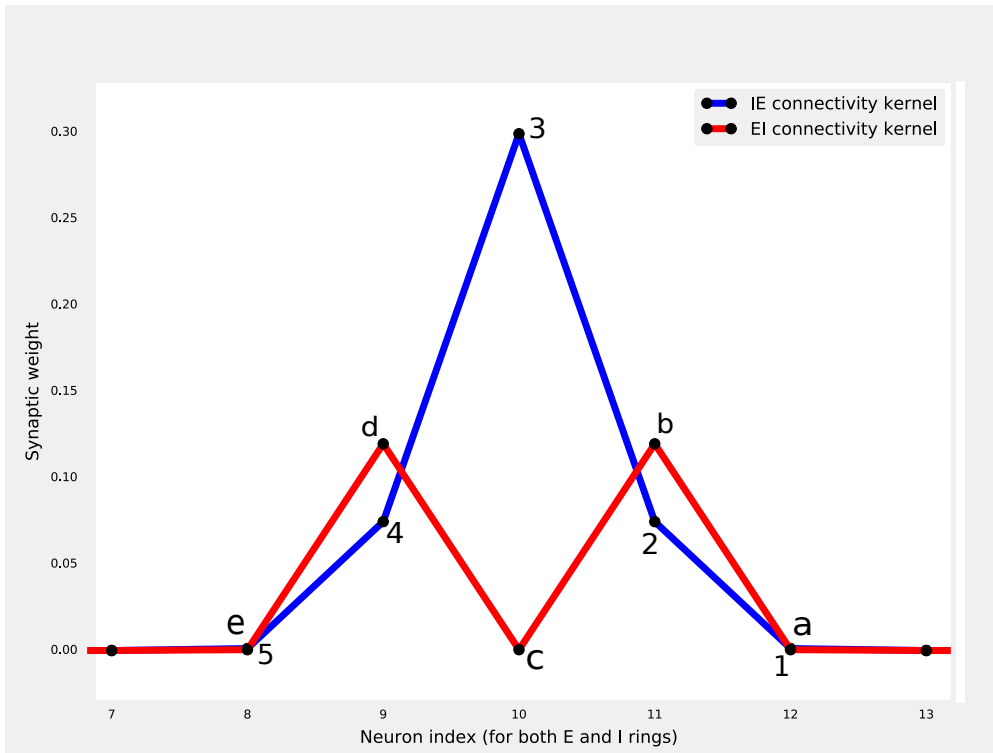


Figure 19. The *IE* and *EI* connectivity kernels for a particular neuron. Both the *IE* and *EI* kernels have been superimposed on each other for the same neuron index (the same position on both *E* and *I* rings). The numbers (1-5) are labels that have been assigned to different postsynaptic neurons on the outgoing *IE* kernel. Similarly, the alphabets (a-e) are positions assigned on the *EI* kernel. The y-axis contains synaptic weight values (mS/cm^2), these values are accurate and are the same values that have been used in the simulations (before STDP).

- **The values of the rate constants and reversal potential of the synapse**

AMPA synapses: $\alpha = 1.1 \text{ msec}^{-1}$, $\beta = 0.19 \text{ msec}^{-1}$, $E_{syn} = 0.0 \text{ mV}$

GABA_A synapses: $\alpha = 10.5 \text{ msec}^{-1}$, $\beta = 0.166 \text{ msec}^{-1}$, $E_{syn} = -80.0 \text{ mV}$

- Duration for which neurotransmitter remains in the synaptic cleft (T_d) = 2.0 msec
- **Maximum values of the postsynaptic conductance (G_{syn}) for different synapses**
There are three types of synapses in the network, viz. *II*, *IE* and *EI* synapses. All the *II* synapses in the network are equivalent, i.e. all the *II* synapses have the same value of $G_{syn} = 1.0 \text{ mS/cm}^2$.
- **Figure 19** shows the outgoing connectivity profile for the same neuron index (10) on both the *E* and *I* rings. The values of maximum postsynaptic conductance for each of these positions is given below. All the values are in mS/cm^2 .

1. *IE connectivity kernel*

Position 1: 0.001157

Position 2: 0.074608

Position 3: 0.299207

Position 4: 0.074608

Position 5: 0.001157

2. *EI connectivity kernel*

Position a: 0.000463

Position b: 0.119683

Position c: 0.000463

Position d: 0.119683

Position e: 0.000463

5.3 STDP parameters

In this section, we will list the parameters used in our simulation of iSTDP in the *IE* synapses of the network [Equation 10]. Figure 8 shows two STDP curves obtained by simulating the pre-post pairing protocol used in Haas, Nowotny, and Abarbanel 2006. Panel **a** of figure 8 has been produced with parameter values that produce an STDP curve that closely resembles that of the Haas, Nowotny, and Abarbanel 2006 experiment. Whereas panel **b** of the figure has been generated with parameter values that give rise to a faster change in network weights. The reasons for having two independent sets of parameter values can be found in section 3.1. The parameter values for both these cases can be found below.

- **Panel a of figure 8**

$$\tau_+ = 5.0 \text{ msec}^{-1}$$

$$\tau_- = 5.0 \text{ msec}^{-1}$$

$$a_+ = 18.0$$

$$a_- = 18.0$$

$$\eta_+ = 0.19$$

$$\eta_- = 0.25$$

$$w_{max} = 3.0 \text{ mS/cm}^2$$

• **Panel b of figure 8**

$$\tau_+ = 74.0 \text{ msec}^{-1}$$

$$\tau_- = 74.0 \text{ msec}^{-1}$$

$$a_+ = 25.0$$

$$a_- = 18.0$$

$$\eta_+ = 0.19$$

$$\eta_- = 0.25$$

$$w_{max} = 3.0 \text{ mS/cm}^2$$

References

- Ahnert, K. and Mulansky, M. (2011). Odeint - Solving ordinary differential equations in C++. AIP Conference Proceedings 1389.1, 1586–1589. ISSN: 0094243X. DOI: 10.1063/1.3637934. arXiv: 1110.3397.
- Assisi, C., Stopfer, M., and Bazhenov, M. (2011). Using the structure of inhibitory networks to unravel mechanisms of spatiotemporal patterning. *Neuron* 69.2, 373–386. ISSN: 08966273. DOI: 10.1016/j.neuron.2010.12.019. arXiv: NIHMS150003. URL: <http://dx.doi.org/10.1016/j.neuron.2010.12.019>.
- Axmacher, N., Elger, C.E., and Fell, J. (2008). Ripples in the medial temporal lobe are relevant for human memory consolidation. *Brain* 131.7, 1806–1817. ISSN: 00068950. DOI: 10.1093/brain/awn103.
- Barry, C., Ginzberg, L.L., et al. (2012). Grid cell firing patterns signal environmental novelty by expansion. *Proceedings of the National Academy of Sciences of the United States of America* 109.43, 17687–92. ISSN: 1091-6490. DOI: 10.1073/pnas.1209918109. arXiv: arXiv:1408.1149. URL: <http://www.pubmedcentral.nih.gov/articlerender.fcgi?artid=3491492%7B%5C%7Dtool=pmcentrez%7B%5C%7Drendertype=abstract>.
- Barry, C., Hayman, R., et al. (2007). Experience-dependent rescaling of entorhinal grids. *Nature neuroscience* 10.6, 682–684. ISSN: 1097-6256. DOI: 10.1038/nn1905.
- Bi, G.Q. and Poo, M.M. (1998). Synaptic modifications in cultured hippocampal neurons: dependence on spike timing, synaptic strength, and postsynaptic cell type. *The Journal of neuroscience : the official journal of the Society for Neuroscience* 18.24, 10464–10472. ISSN: 0270-6474. DOI: 10.1038/25665.
- Blair, H.T., Gupta, K., and Zhang, K. (2008). Conversion of a phase- to a rate-coded position signal by a three-stage model of theta cells, grid cells, and place cells. *Hippocampus* 18.12, 1239–1255. ISSN: 10509631. DOI: 10.1002/hipo.20509. arXiv: NIHMS150003.
- Bliss, T.V.P. and Lømo, T. (1973). Long-lasting potentiation of synaptic transmission in the dentate area of the anaesthetized rabbit following stimulation of the perforant path. *The Journal of Physiology* 232.2, 331–356. ISSN: 14697793. DOI: 10.1113/jphysiol.1973.sp010273.
- Bliss, T.V. and Collingridge, G.L. (1993). A synaptic model of memory: long-term potentiation in the hippocampus. *Nature* 361.6407, 31–39. ISSN: 0028-0836. DOI: 10.1038/361031a0. arXiv: 0402594v3 [arXiv:cond-mat].
- Buhry, L., Azizi, A.H., and Cheng, S. (2011). Reactivation, replay, and preplay: How it might all fit together. *Neural Plasticity* 2011. ISSN: 16875443. DOI: 10.1155/2011/203462.

Burak, Y. and Fiete, I.R. (2009). Accurate path integration in continuous attractor network models of grid cells. *PLoS Computational Biology* 5.2. ISSN: 1553734X. DOI: 10.1371/journal.pcbi.1000291. arXiv: 0811.1826.

Buzsáki, G. (2015). Hippocampal sharp wave-ripple: A cognitive biomarker for episodic memory and planning. *Hippocampus* 25.10, 1073–1188. ISSN: 10981063. DOI: 10.1002/hipo.22488. arXiv: arXiv:1011.1669v3.

Couey, J.J. et al. (2013). Recurrent inhibitory circuitry as a mechanism for grid formation. *Nature neuroscience* 16.3, 318–24. ISSN: 1546-1726. DOI: 10.1038/nn.3310. URL: <http://www.ncbi.nlm.nih.gov/pubmed/23334580>.

Deuker, L. et al. (2016). An event map of memory space in the hippocampus. *eLife* 5.OCTOBER2016, 1–26. ISSN: 2050084X. DOI: 10.7554/eLife.21263.

Diba, K. and Buzsáki, G. (2007). Forward and reverse hippocampal place-cell sequences during ripples. *Nature Neuroscience* 10.10, 1241–1242. ISSN: 10976256. DOI: 10.1038/nn1961. arXiv: NIHMS150003.

Dickson, C.T. et al. (2000). Properties and role of I(h) in the pacing of subthreshold oscillations in entorhinal cortex layer II neurons. *Journal of neurophysiology* 83.5, 2562–2579. ISSN: 0022-3077. DOI: 10.220.32.247.

Doeller, C.F., Barry, C., and Burgess, N. (2010). Evidence for grid cells in a human memory network. *Nature* 463.7281, 657–661. ISSN: 00280836. DOI: 10.1038/nature08704. arXiv: arXiv:1011.1669v3. URL: <http://dx.doi.org/10.1038/nature08704>.

Dupret, D. et al. (2010). The reorganization and reactivation of hippocampal maps predict spatial memory performance. *Nature Neuroscience* 13.8, 995–1002. ISSN: 10976256. DOI: 10.1038/nn.2599. URL: <http://dx.doi.org/10.1038/nn.2599>.

Ego-Stengel, V. and Wilson, M.A. (2010). Disruption of ripple-associated hippocampal activity during rest impairs spatial learning in the rat. *Hippocampus* 20.1, 1–10. ISSN: 10509631. DOI: 10.1002/hipo.20707.

Feldman, D.E. (2012). The Spike-Timing Dependence of Plasticity. *Neuron* 75.4, 556–571. ISSN: 08966273. DOI: 10.1016/j.neuron.2012.08.001.

Fransén, E. et al. (2004). Ionic mechanisms in the generation of subthreshold oscillations and action potential clustering in entorhinal layer II stellate neurons. *Hippocampus* 14.3, 368–384. ISSN: 10509631. DOI: 10.1002/hipo.10198.

Giocomo, L.M., Moser, M.B., and Moser, E.I. (2011). Computational models of grid cells. *Neuron* 71.4, 589–603. ISSN: 08966273. DOI: 10.1016/j.neuron.2011.07.023. URL: <http://dx.doi.org/10.1016/j.neuron.2011.07.023>.

Girardeau, G. et al. (2009). Selective suppression of hippocampal ripples impairs spatial memory. *Nature Neuroscience* 12.10, 1222–1223. ISSN: 10976256. DOI: 10.1038/nn.2384. URL: <http://dx.doi.org/10.1038/nn.2384>.

Gonzalez-Sulser, A. et al. (2014). GABAergic Projections from the Medial Septum Selectively Inhibit Interneurons in the Medial Entorhinal Cortex. *Journal of Neuroscience* 34.50, 16739–16743. ISSN: 0270-6474. DOI: 10.1523/JNEUROSCI.1612-14.2014. URL: <http://www.jneurosci.org/cgi/doi/10.1523/JNEUROSCI.1612-14.2014>.

Haas, J.S., Nowotny, T., and Abarbanel, H.D.I. (2006). Spike-timing-dependent plasticity of inhibitory synapses in the entorhinal cortex. *J Neurophysiol* 96, 3305–3313. ISSN: 0022-3077. DOI: 10.1152/jn.00551.2006. URL: <http://dx.doi.org/10.1152/jn.00551.2006>.

Hafting, T. et al. (2005). Microstructure of a spatial map in the entorhinal cortex. *Nature* 436.7052, 801–806. ISSN: 0028-0836. DOI: 10.1038/nature03721. arXiv: [/dx.doi.org/10.1038/nature01964](http://dx.doi.org/10.1038/nature01964) [http:].

Hasselmo, M.E. and Shay, C.F. (2014). Grid cell firing patterns may arise from feedback interaction between intrinsic rebound spiking and transverse traveling waves with multiple heading angles. *Frontiers in Systems Neuroscience* 8.October, 201. ISSN: 1662-5137. DOI: 10.3389/fnsys.2014.00201. URL: <http://journal.frontiersin.org/article/10.3389/fnsys.2014.00201/abstract>.

Jadhav, S.P. et al. (2012). Reports Awake Hippocampal Sharp-Wave Ripples Support Spatial Memory. *May*, 1–5. ISSN: 0036-8075, 1095-9203. DOI: 10.1126/science.1217230.

Jeewajee, A. et al. (2008). Environmental novelty is signaled by reduction of the hippocampal theta frequency. *Hippocampus* 18.4, 340–348. ISSN: 10509631. DOI: 10.1002/hipo.20394.

Koenig, J. (2011). The Spatial Periodicity of Grid Cells. *Science* 592.Issue: 6029, 592–595. ISSN: 1095-9203. DOI: 10.1126/science.1201685.

Krupic, J. et al. (2015). Grid cell symmetry is shaped by environmental geometry. *Nature* 518.7538, 232–235. ISSN: 14764687. DOI: 10.1038/nature14153. URL: <http://dx.doi.org/10.1038/nature14153>.

Louie, K. and Wilson, M.A. (2001). Temporally structured replay of awake hippocampal ensemble activity during rapid eye movement sleep. *Neuron* 29.1, 145–156. ISSN: 08966273. DOI: 10.1016/S0896-6273(01)00186-6.

Markram, H. et al. (1997). Regulation of synaptic efficacy by coincidence of postsynaptic APs and EPSPs. *Science* 275.January, 213–215.

Martin, S.J., Grimwood, P.D., and Morris, R.G.M. (2000). Synaptic plasticity and memory: An Evaluation of the Hypothesis. *Annual review of neuroscience Hebb* 1949, 649–711. ISSN: 0147-006X. DOI: 10.1146/annurev.neuro.23.1.649. arXiv: arXiv:1011.1669v3.

- Morrison, A., Diesmann, M., and Gerstner, W. (2008). Phenomenological models of synaptic plasticity based on spike timing. *Biological Cybernetics* 98.6, 459–478. ISSN: 03401200. DOI: 10.1007/s00422-008-0233-1.
- Moser, E.I., Moser, M.-B., and McNaughton, B.L. (2017). Spatial representation in the hippocampal formation: a history. *Nature Neuroscience* 20.11, 1448–1464. ISSN: 1097-6256. DOI: 10.1038/nn.4653. URL: <http://www.nature.com/doifinder/10.1038/nn.4653>.
- Moser, E.I., Roudi, Y., et al. (2014). Grid cells and cortical representation. *Nature Reviews Neuroscience* 15.7, 466–481. ISSN: 1471-0048. DOI: 10.1038/nrn3766. URL: <http://eutils.ncbi.nlm.nih.gov/entrez/eutils/elink.fcgi?dbfrom=pubmed%7B%5C%7Ddid=24917300%7B%5C%7Dretmode=ref%7B%5C%7Dcmd=prlinks%7B%5C%7D5Cnpapers3://publication/doi/10.1038/nrn3766>.
- Mulansky, M. and Kreuz, T. (2016). PySpike—A Python library for analyzing spike train synchrony. *SoftwareX* 5, 183–189. ISSN: 23527110. DOI: 10.1016/j.softx.2016.07.006. arXiv: 1603.03293. URL: <http://dx.doi.org/10.1016/j.softx.2016.07.006>.
- O’Keefe, J. and Dostrovsky, J. (1971). The hippocampus as a spatial map. Preliminary evidence from unit activity in the freely-moving rat. *Brain Research* 34.1, 171–175. ISSN: 00068993. DOI: 10.1016/0006-8993(71)90358-1.
- O’Keefe, J. and Burgess, N. (2005). Dual phase and rate coding in hippocampal place cells: Theoretical significance and relationship to entorhinal grid cells. *Hippocampus* 15.7, 853–866. ISSN: 10509631. DOI: 10.1002/hipo.20115.
- Pavlidis, C. and Winson, J. (1989). Influences of hippocampal place cell firing in the awake state on the activity of these cells during subsequent sleep episodes. *The Journal of neuroscience* 9.8, 2907–2918. ISSN: 0270-6474. DOI: 10.1523/jneurosci.4342-04.2005.
- Rotstein, H.G. et al. (2006). The dynamic structure underlying subthreshold oscillatory activity and the onset of spikes in a model of medial entorhinal cortex stellate cells. *Journal of Computational Neuroscience* 21.3, 271–292. ISSN: 09295313. DOI: 10.1007/s10827-006-8096-8.
- Schmidt, H. et al. (2017). Axonal synapse sorting in medial entorhinal cortex. *Nature* 549.7673, 469–475. ISSN: 0028-0836. DOI: 10.1038/nature24005. URL: <http://www.nature.com/doifinder/10.1038/nature24005>.
- Sjöström, P.J., Turrigiano, G.G., and Nelson, S.B. (2001). Rate, timing, and cooperativity jointly determine cortical synaptic plasticity. *Neuron* 32.6, 1149–1164. ISSN: 08966273. DOI: 10.1016/S0896-6273(01)00542-6.
- Skaggs, W.E. and McNaughton, B.L. (1996). Replay of Neuronal Firing Sequences in Rat Hippocampus During Sleep Following Spatial Experience. *Science* 271.5257,

1870–1873. ISSN: 0036-8075. DOI: 10.1126/science.271.5257.1870. URL: <http://www.sciencemag.org/cgi/doi/10.1126/science.271.5257.1870>.

Taube, J.S., Muller, R.U., and Ranck, J.B. (1990). Head-direction cells recorded from the postsubiculum in freely moving rats. I. Description and quantitative analysis. *The Journal of neuroscience : the official journal of the Society for Neuroscience* 10.2, 420–35. ISSN: 0270-6474. DOI: 10.1212/01.wnl.0000299117.48935.2e. URL: <http://www.ncbi.nlm.nih.gov/pubmed/2303851>.

Taube, J.S., Muller, R.U., and Ranck JB, J.B. (1990). Head-direction cells recorded from the postsubiculum in freely moving rats. II. Effects of environmental manipulations. *J. Neurosci.* 10.2, 436–447. ISSN: 0270-6474. DOI: 10.1212/01.wnl.0000299117.48935.2e. URL: <http://www.jneurosci.org/content/10/2/436.short%7B%5C%7D5Cnhttp://www.ncbi.nlm.nih.gov/pubmed/2303852>.

Tolman, E.C. (1948). Cognitive maps in rats and men. *Psychological Review* 55.4, 189–208. ISSN: 0033295X. DOI: 10.1037/h0061626. arXiv: h0054651 [10.1037].

Vogels, T.P. et al. (2013). Inhibitory synaptic plasticity: spike timing-dependence and putative network function. *Frontiers in Neural Circuits* 7.July, 1–11. ISSN: 1662-5110. DOI: 10.3389/fncir.2013.00119. URL: <http://journal.frontiersin.org/article/10.3389/fncir.2013.00119/abstract>.

Xiao-Jing Wang and György Buzsáki (1996). Gamma Oscillation by Synaptic Inhibition in a Hippocampal Interneuronal Network Model. *The Journal of Neuroscience* 16.20, 6402–6413. ISSN: 0270-6474. DOI: citeulike-article-id:134404. URL: <http://www.jneurosci.org/content/16/20/6402.short>.

Yartsev, M.M., Witter, M.P., and Ulanovsky, N. (2011). Grid cells without theta oscillations in the entorhinal cortex of bats. *Nature* 479.7371, 103–107. ISSN: 00280836. DOI: 10.1038/nature10583. URL: <http://dx.doi.org/10.1038/nature10583>.

Yassa, M.A. (2018). Brain Rhythms: Higher-Frequency Theta Oscillations Make Sense in Moving Humans. *Current Biology* 28.2, R70–R72. ISSN: 09609822. DOI: 10.1016/j.cub.2017.11.045. URL: <http://linkinghub.elsevier.com/retrieve/pii/S0960982217315270>.